GEOLOGICA CARPATHICA, DECEMBER 2015, 66, 6, 499–514 doi: 10.1515/geoca-2015-0041

Orthopyroxene-enrichment in the lherzolite-websterite xenolith suite from Paleogene alkali basalts of the Poiana Ruscă Mountains (Romania)

ZSUZSANNA NÉDLI[1], CSABA SZABÓ[1]✉ and JÚLIA DÉGI[2]

[1]Lithosphere Fluid Research Lab, Department of Petrology and Geochemistry, Eötvös University, Pázmány Péter setány 1/C, H-1117 Budapest, Hungary; nedlizs@yahoo.com; ✉cszabo@elte.hu
[2]Geological and Geophysical Institute of Hungary, Stefánia út 14, H-1143 Budapest, Hungary; degi.julia@mfgi.hu

(Manuscript received March 17, 2015; accepted in revised form August 10, 2015)

Abstract: In this paper we present the petrography and geochemistry of a recently collected lherzolite-websterite xenolith series and of clinopyroxene xenocrysts, hosted in Upper Cretaceous–Paleogene basanites of Poiana Ruscă (Romania), whose xenoliths show notable orthopyroxene-enrichment. In the series a slightly deformed porphyroclastic-equigranular textured series could represent the early mantle characteristics, and in many cases notable orthopyroxene growth and poikilitic texture formation was observed. The most abundant mantle lithology, Type A xenoliths have high Al- and Na-contents but low mg# of the pyroxenes and low cr# of spinel suggesting a low degree (< 10 %) of mafic melt removal. They are also generally poor in overall REE-s (rare earth elements) and have flat REY (rare earth elements + Y) patterns with slight LREE-depletion. The geochemistry of the Type A xenoliths and calculated melt composition in equilibrium with the xenolith clinopyroxenes suggests that the percolating melt causing the poikilitization can be linked to a mafic, Al-Na-rich, volatile-poor melt and show similarity with the Late Cretaceous–Paleogene (66–72 Ma) subduction-related andesitic magmatism of Poiana Ruscă. Type B xenoliths, with their slightly different chemistry, suggest that, after the ancient depletion, the mantle went through a slight metasomatic event. A subsequent passage of mafic melts in the mantle, with similar compositions to the older andesitic magmatism of Poiana Ruscă, is recorded in the pyroxenites (Fe-rich xenoliths), whereas the megacrysts seem to be cogenetic with the host basanite. The Poiana Ruscă xenoliths differ from the orthopyroxene-enriched mantle xenoliths described previously from the Carpathian-Pannonian Region and from the Dacia block.

Key words: Paleogene, S Carpathians, mantle xenolith petrology, geochemistry, alkali basalt.

Introduction

Orthopyroxene-rich xenoliths represent only a minor part of the lithospheric mantle lithologies (Downes 2001). After earlier interpretation as mantle residues after extensive melt extraction (Ringwood 1958), several different processes have been proposed more recently to explain their formation. These interpretations suggest that orthopyroxene-rich lithologies can be (1) products of interaction between mantle wall rock and aqueous SiO_2-rich melts/fluids derived from slab dehydration or melting (e.g. Kelemen et al. 1992; Arai et al. 2003, 2004), (2) reaction products of interaction between mantle wall rock and silica-rich melts of alkali basaltic origin percolating in the mantle (e.g. Arai et al. 2006; Dantas et al. 2009), (3) mafic-ultramafic cumulates crystallized at mantle depth (Embey-Isztin et al. 1989; Santos et al. 2002; Cvetković et al. 2004, 2007; Bali et al. 2007) and (4) products of infiltration-crystallization-reaction processes (Wulff-Pedersen et al. 1996, 1999).

These rocks have been described from several localities of the Carpathian-Pannonian-Balkan Region (Embey-Isztin et al. 1989, 2001; Cvetković et al. 2004, 2007; Bali et al. 2007, 2008; Marchev et al. 2008; Embey-Isztin & Dobosi 2011; Berkesi et al. 2012) and show wide variations. Some studies have proposed the origin of these orthopyroxene-enriched rocks as mantle-depth crystallization products from boninitic melts (Embey-Isztin et al. 1989; Cvetković et al. 2007; Bali et al. 2007, 2008). Some recent papers (Cvetković et al. 2004, 2010; Embey-Isztin & Dobosi 2011) suggested the possibility of orthopyroxene-rich (poikilitic) lithologies as resulting from magmatic modification of the lithospheric mantle via infiltrating (alkaline) mafic melt.

In this paper we present the petrography and geochemistry of a recently collected lherzolite-websterite xenolith series and of clinopyroxene xenocrysts, hosted in Upper Cretaceous–Paleogene basanites of Poiana Ruscă (Romania), whose xenoliths show notable orthopyroxene-enrichment. We discuss the main characteristics of the lithospheric mantle beneath the region and explain what processes may be responsible for the orthopyroxene-enrichment of the studied mantle, which seems to be rather different in geochemical features and origin from the orthopyroxene-enriched xenoliths of the Carpathian-Pannonian-Balkan Region described earlier.

Geological background

The Poiana Ruscă Mountains (Romania) are situated in the South Carpathians and are largely composed of a low-grade metamorphic volcano-sedimentary series of Devonian–Lower Carboniferous age, related to the Rhenohercynian Zone of

Central-Western Europe (Kräutner 1997). These rocks were strongly deformed and metamorphosed during the Variscan orogeny in Carboniferous time and were also involved in mid-Cretaceous thrusting of the Supragetic unit of the South Carpathians (e.g. Iancu et al. 2005).

During the Mesozoic collision of the African and Eurasian plates and a number of smaller continental microplates, the region was dominated by the closure of the western branch of the Vardar Zone and eastward/north-eastward subduction of the Tethyan oceanic lithosphere beneath stable Europe (e.g. Ianovici et al. 1977; Karamata et al. 1997). This tectonic event created a 1000 km long belt of Late Cretaceous–Early Paleogene arc intrusive rocks, regionally referred to as banatites (von Cotta 1864) or as the Banatite-Timok-Srednjegorie Magmatic and Metallogenetic Belt (Berza et al. 1998), and volcano-sedimentary successions, appearing throughout the basement of the SW-Carpathians (Banat, Poiana Ruscă, Fig. 1) and Apuseni Mts (Ciobanu et al. 2002). The geochemistry of the banatitic magmatic suites shows an alkaline to calc-alkaline signature and suggests subduction-related magma generation (Rădulescu & Săndulescu 1973; Russo-Săndulescu et al. 1978; Russo-Săndulescu & Berza 1979; Downes et al. 1995; Berza et al. 1998).

Kräutner (1969) presented the first detailed description of the sub-volcanic alkaline basaltic bodies outcropping in the Poiana Ruscă massif, south of the Apuseni Mts, which postdated the banatitic magmatic suites. He divided the magmatic rocks geographically and geochemically into six groups. Downes et al. (1995) reported K-Ar data, petrography and geochemistry of the alkaline rocks and the first petrologic and geochemical data on their mantle xenoliths. They concluded that the Late Cretaceous–Paleogene magma emplacement occurred in two phases. The older (66–72 Ma) andesitic magmas could have been formed by subduction-related volcanism, from a mantle source enriched by previous subduction. The andesitic magmatism was followed by alkaline basic volcanism (48–58 Ma), probably related to deep lithospheric fractures at the boundary between the Tisza and Dacia terrains (Downes et al. 1995). Regarding the mantle xenoliths, Downes et al. (1995) summarized that they represent a generally unmetasomatized, slightly deformed mantle section and the rare occurrence of pyroxenites suggests the passage of mafic magmas through the lithospheric mantle. Recently Tshegg et al. (2010) studied the younger basanitic activity of Poiana Ruscă and concluded that its magmatics were formed by a low fraction melting of a slightly CO_2 influenced garnet-facies OIB-like asthenospheric source. The magmatic activity can be related to a post-collision extensional tectonic event, similar to the Paleocene–Eocene magmatic activity which generated the xenolith-bearing East Serbian mafic alkaline magmatic rocks (ES-MAR) (Cvetković et al. 2013).

These Serbian Paleogene mafic alkaline rocks (Fig. 1) form a north–south line within the Carpatho-Balkan tectonic terrain as a continuation of the volcanic chain of the Apuseni Mts (Cvetković et al. 2004). Jovanović et al. (2001) and Cvetković et al. (2004, 2007, 2010, 2013) presented detailed descriptions of the magmatism and the mantle xenoliths. They suggested that the lithospheric mantle underneath East Serbia is more depleted than the normal European lithosphere and described two different types of orthopyroxene-rich lithologies. The first

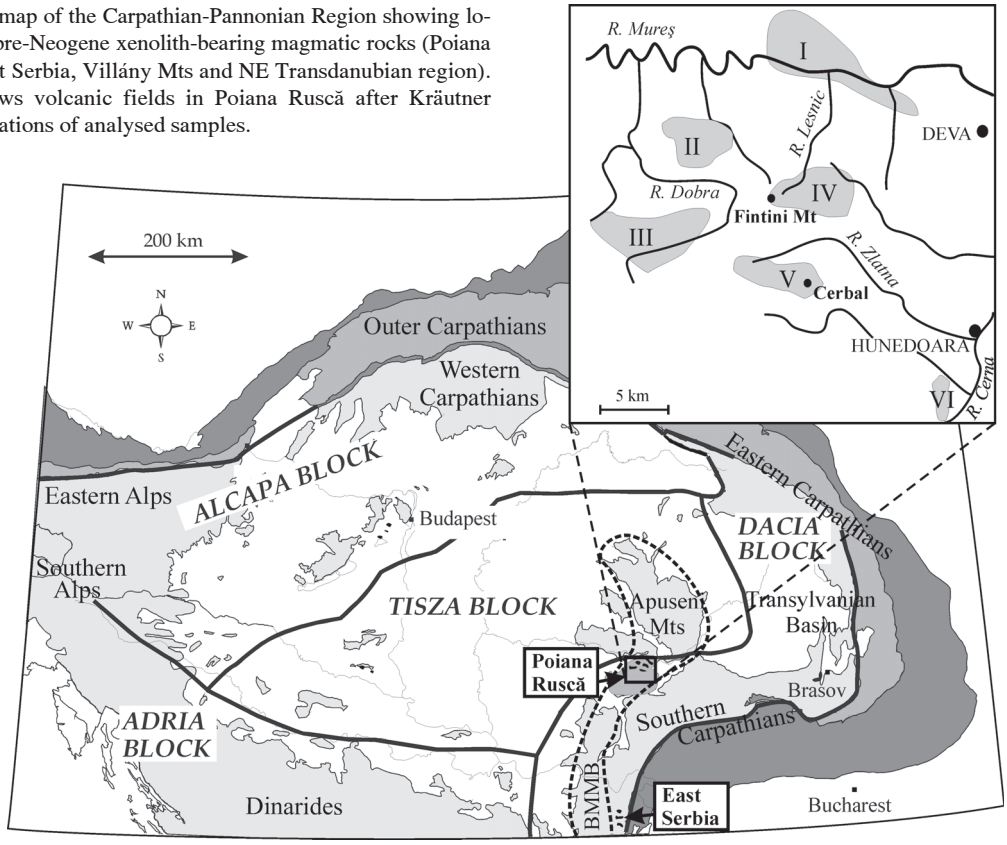

Fig. 1. Sketch map of the Carpathian-Pannonian Region showing localities of the pre-Neogene xenolith-bearing magmatic rocks (Poiana Ruscă and East Serbia, Villány Mts and NE Transdanubian region). The inset shows volcanic fields in Poiana Ruscă after Kräutner (1969) and locations of analysed samples.

type of websterites was interpreted by interaction with percolating mafic alkaline melts (Cvetković et al. 2004), the second type in relation to crystallization of subduction-related presumably boninitic melts (Cvetković et al. 2007).

Marchev et al. (2006, 2008) also described a pyroxene-rich mantle xenolith suite from the Oligocene alkali basalt-lamprophyre series as underplated cumulate rocks. A trace element study of the most primitive cumulate rocks indicates that they formed from a mantle-derived parent melt similar to their host alkaline magma. The orthopyroxenite and websterite xenoliths are believed to have been formed from the same, but more fractionated, melt which may have had a Mg-Si-rich alkali-basaltic character.

Analytical methods

Xenolith-bearing basanite samples were collected from the Cerbal and Fintini Mt localities (Fig. 1). From the largest xenoliths, 17 double-polished thick sections were prepared for petrographic description and modal composition estimations. The modal composition of the xenoliths was approximated by digital image analysis of high resolution scanning of whole thick sections, in the majority of cases including all the xenolith, using the image analysis software package of Corel X4. The modal proportion of minerals is expressed as the percentage per total area of rock surface corrected for grain boundaries. The validity of the calculated modal compositions was checked under an optical microscope. The petrographic study was carried out at the Lithosphere Fluid Research Lab, Eötvös University (Budapest, Hungary) using a Nikon Eclipse E600 POL polarized light microscope.

The microprobe analysis was carried out on representative thin-sections with a Cameca SX100 Electron Microprobe at the Natural History Museum, London. Data were collected at 15 kV, 20 nA beam current, for 100 s per analysis, using a Bruker AXS 4010 XFlash silicon drift energy dispersive X-ray (EDX) detector and 1 μm spot diameter. Natural and synthetic minerals were used as standards. Concentrations were averaged from 2–4 measurements, core to rim homogeneity was checked and outer rim measurement was avoided.

Laser ICP-MS trace element analysis of silicate phases (clinopyroxene, orthopyroxene and olivine) was performed at the Natural History Museum, London. The LA-ICP-MS system consists of an Agilent 7500cs quadrupole ICP-MS, coupled to a New Wave Research UP193FX excimer laser. The synthetic glass reference material NIST 612 was used as the calibration standard, using the average composition of Pearce et al. (1997). Calcium (^{44}Ca) was used as the internal standard for quantification of analysis. The raw data was processed using the offline Lamtrace software. Trace element concentrations were averaged from 2–4 measurements.

Petrography

Xenoliths were collected from two xenolith-bearing basanite localities in Poiana Ruscă: most of the samples are from near Cerbal and some samples from Fintini Mt (Fig. 1). The xenoliths are fresh, their sizes are 1.5–5.0 cm, and they show variability in modal composition and texture. They vary widely between olivine-rich wehrlite, lherzolite and orthopyroxene-rich olivine websterite compositions (Table 1, Fig. 2). One dunite xenolith was also identified. The most distinctive feature of the modal composition is the high variability in orthopyroxene content (1–45 vol. %). No OH-bearing minerals were found in any xenoliths.

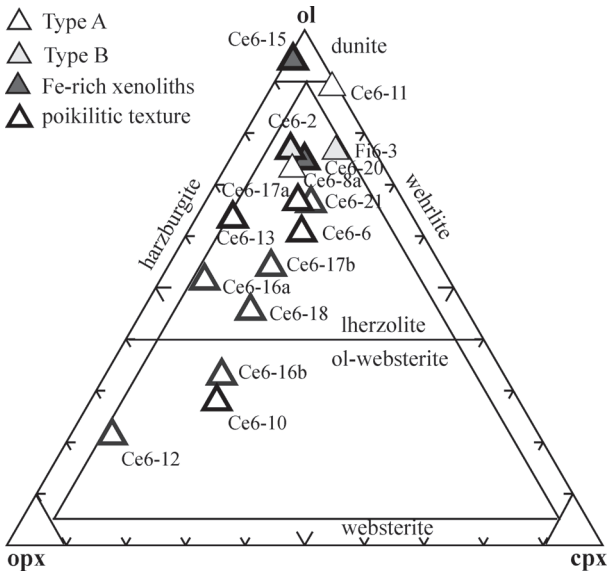

Fig. 2. Modal composition of xenoliths from Poiana Ruscă.

Table 1: Modal composition, textures, and equilibrium temperatures of the Poiana Ruscă xenoliths. **T(°C)** — after Brey & Köhler (1990) cpx-opx equilibrium T, **fO_2** — after Ballhaus et al. (1991).

Sample	Rock type	Texture	Modal composition	Type	Equilibrium	
					T(°C)	fO_2
Ce6-8a	lherzolite	porphy-equiranular	ol: 71; opx: 15; cpx: 11; sp: 3	A	950	–0.55
Ce6-10a	ol websterite	poikilitic	ol: 28; opx: 52; cpx: 18; sp: 2	A	1020	–0.12
Ce6-11a	wherlite	porphy-equiranular	ol: 87; opx: 1; cpx: 10; sp: 2	A	1000	–0.48
Ce6-16a	lherzolite	poikilitic	ol: 50; opx: 40; cpx: 7; sp: 3	A	1000	–1.46
Ce6-16b	ol websterite	poikilitic	ol: 32; opx: 47; cpx: 19; sp: 2	A	1010	–1,15
Ca6-17a	lherzolite	poikilitic	ol: 67; opx: 17; cpx: 14; sp: 2	A	960	–0.93
Ce6-17b	lherzolite	poikilitic	ol: 51; opx: 27; cpx: 16; sp: 6	A	970	–0.53
Ce6-18	lherzolite	poikilitic	ol: 45; opx: 36; cpx: 18; sp: 1	A	990	0.17
Ce6-21	lherzolite	poikilitic	ol: 63; opx: 14; cpx: 16; sp: 7	A	990	–0.52
Ce6-12	ol websterite	poikilitic	ol: 21; opx: 71; cpx: 7; sp: 1	A	960	–0.71
Ce6-13	lherzolite	poikilitic	ol: 66; opx: 27; cpx: 5; sp: 2	A	930	–0.72
Ce6-2	lherzolite	poikilitic	ol: 78; opx: 14; cpx: 7; sp: 1	B	1110	2.95
Fi6-3	lherzolite	porphy-equiranular	ol: 78; opx: 5; cpx: 15; sp: 2	B	980	–0.94
Ce6-20	lherzolite	poikilitic	ol: 73; opx: 13; cpx: 11; sp: 3	Fe-rich	900	0.42
Ce6-15	dunite	poikilitic	ol: 84; opx: 6; cpx: 2; sp: 8	Fe-rich	900	0.35
Ce6-7	megacryst		cpx			
Ce6-11a	megacryst		cpx			

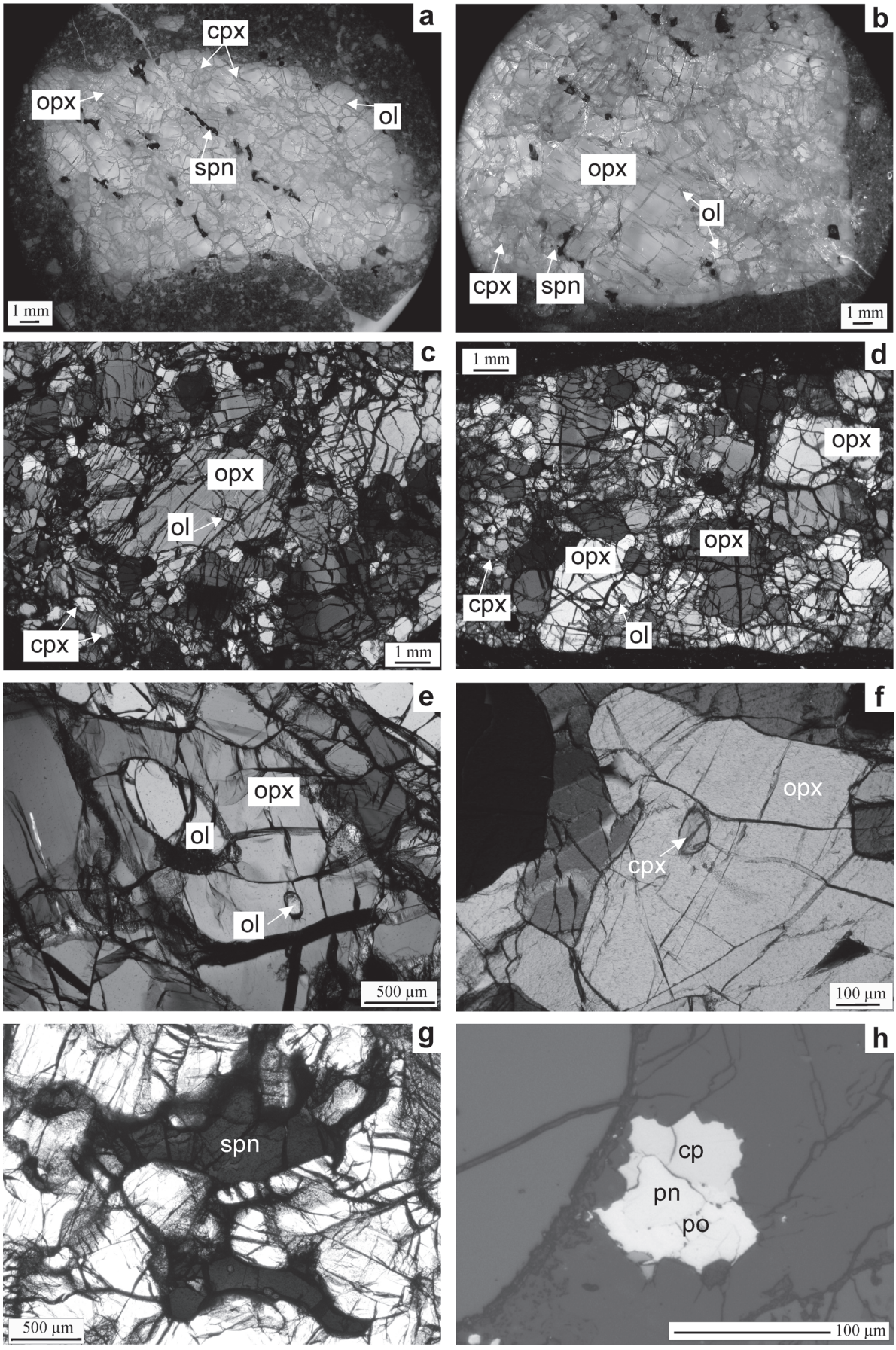
a
cpx
opx
ol
spn
1 mm
b
opx
ol
cpx
spn
1 mm
c
opx
ol
cpx
1 mm
d
1 mm
opx
opx
opx
cpx
ol
e
opx
ol
ol
500 µm
f
opx
cpx
100 µm
g
spn
500 µm
h
cp
pn
po
100 µm

Two main groups can be distinguished on the basis of texture: a transitional porphyroclastic-equigranular textured and a poikilitic textured group. In **porphyroclastic-equigranular** textured xenoliths the grain size is variable, olivines are typically larger (2–10 mm) than pyroxenes (1–5 mm). The large olivine grains often show polygonization and recrystallization into smaller aggregates, sometimes subgrain rotation is also observed. The aggregates are then nearly mosaic-shaped. They often present a weak mineral lineation in texture with slightly elongated (mostly olivine) grains and subgrains and a well-defined linear arrangement of (mostly) spinel grains. Spinels are small and holly-leaf shaped or rounded, often linearly arranged parallel to the elongation of olivine grains (Fig. 3a). Spinel frequently occurs also as inclusion in silicate minerals. The constituent minerals show straight grain boundaries and triple junctions.

Most of the samples belong to the **poikilitic** textured group characterized by coarse or bimodal grain size (Fig. 3b,c,d) and

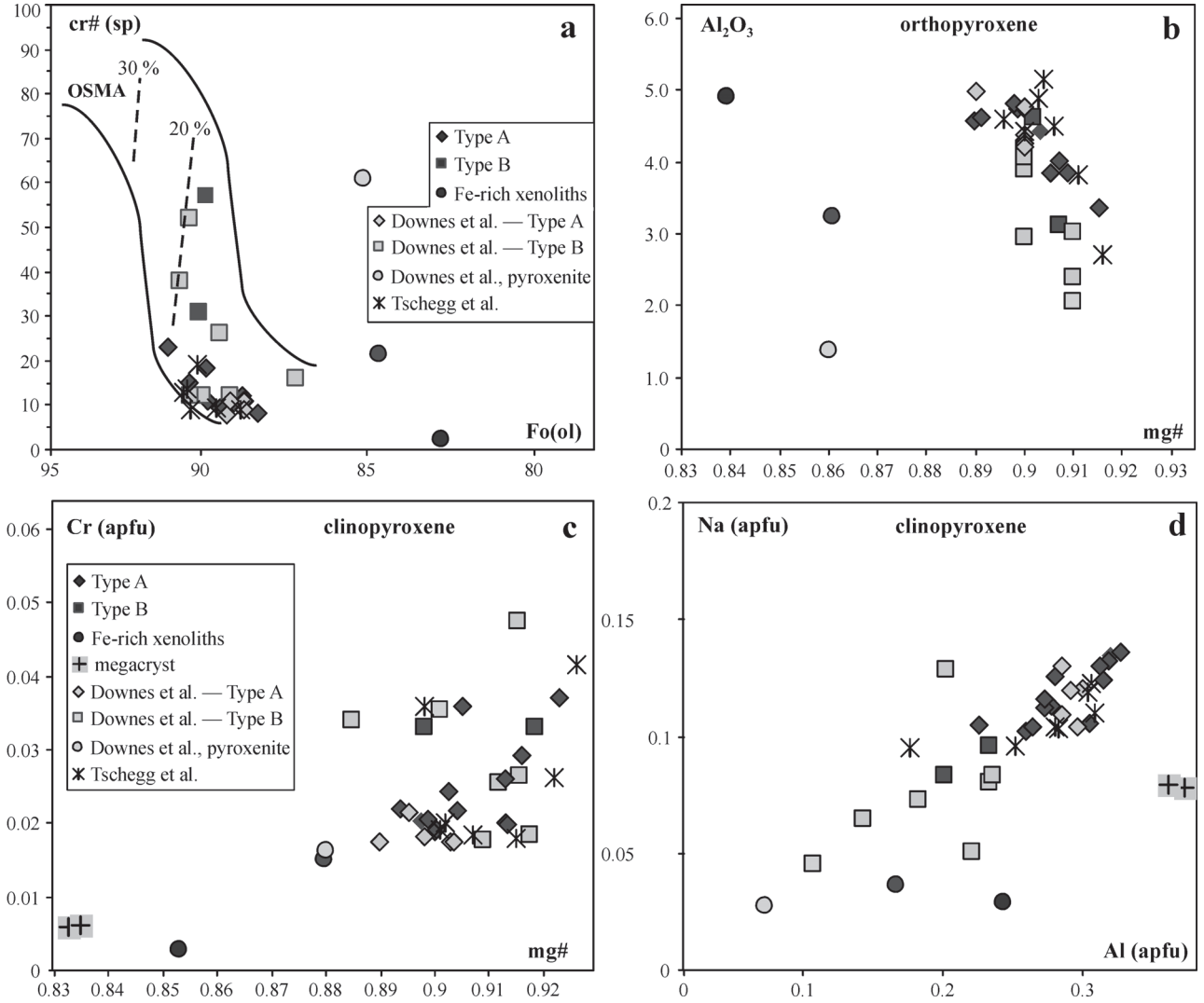

Fig. 4. Mineral chemistry of the studied xenoliths. Previously studied xenoliths from the same area/localities (Downes et al. 1995; Tschegg et al. 2010) are also presented for comparison. Groups "Downes et al. — Type A" and "Downes et al. — Type B" are proposed by this study based on the similarity of these samples in mineral chemistry to the samples analysed in this study. **a** — distribution of the samples on the olivine-spinel mantle array "OSMA" proposed by Arai (1994), dashed lines indicate the extent of depletion of xenoliths (Arai 1994); **b** — mg# vs. Al_2O_3 in orthopyroxenes; **c** — mg# vs. Cr (apfu) in clinopyroxenes; **d** — Al (apfu) vs. Na (apfu) in clinopyroxenes.

Fig. 3. Photomicrographs (ol = olivine, opx = orthopyroxene, cpx = clinopyroxene, cp = chalcopyrite, pn = pentlandite, po = pyrrhotite). **a** — xenolith Ce6-11, wehrlite, linear arrangement of spinel among silicate minerals; **b** — xenolith Ce6-16b, poikilitic textured olivine websterite, with large orthopyroxene porphyroclast in the middle; **c** — xenolith Ce6-17, lherzolite, bimodal grain size in typical poikilitic texture; **d** — xenolith Ce6-20, lherzolite, large orthopyroxene grains in poikilitic texture; **e** — xenolith Ce6-12, olivine websterite, olivine inclusions in orthopyroxene porphyroclast; **f** — xenolith Ce6-16b, poikilitic textured olivine websterite, orthopyroxene porphyroclast includes clynopyroxene; **g** — xenolith Ce6-16b, poikilitic textured olivine websterite, vermicular spinel; **h** — xenolith Ce6-15, dunite, sulphide inclusion.

the presence of various solid inclusions in silicate phases (Fig. 3c,e,f). Orthopyroxene has a typically larger grain size (up to 3–4 mm) than the other minerals (Fig. 3b,c,d) and often encloses olivine and rare clinopyroxene (Fig. 3e,f). Two different grain boundaries are characteristic in the same xenolith: pyroxenes, particularly orthopyroxenes, have mostly curvilinear boundaries but, close to these grains, straight boundaries and triple junctions are also observed among smaller minerals

Table 2: Olivine major element data of the studied Poiana Ruscă xenoliths.

Sample	Ce6-8a	Ce6-10a	Ce6-11a	Ce6-16a	Ce6-16b	Ce6-17a	Ce6-17b	Ce6-18	Ce6-21	Ce6-12	Ce6-13	Ce6-2	Fi6-3	Ce6-15	Ce6-20
Type	**A**	**A**	**A**	**A**	**A**	**A**	**A**	**A**	**A**	**A**	**A**	**B**	**B**	**Fe-rich**	**Fe-rich**
(wt. %)															
SiO_2	40.57	40.36	40.72	40.57	40.52	40.42	40.86	40.33	40.73	40.52	40.62	40.46	40.94	39.42	39.71
TiO_2	0.00	0.00	0.00	0.01	0.00	0.00	0.00	0.01	0.01	0.00	0.00	0.01	0.00	0.00	0.02
Al_2O_3	0.01	0.01	0.00	0.01	0.01	0.00	0.00	0.02	0.00	0.01	0.00	0.01	0.00	0.01	0.00
Cr_2O_3	0.02	0.01	0.03	0.02	0.02	0.02	0.01	0.02	0.01	0.01	0.01	0.03	0.01	0.00	0.01
FeO	9.95	10.45	9.91	10.41	10.29	11.35	8.81	10.91	10.42	9.43	9.69	9.88	9.75	16.24	14.60
MnO	0.15	0.16	0.14	0.12	0.15	0.17	0.13	0.14	0.16	0.13	0.15	0.16	0.16	0.22	0.16
NiO	0.38	0.37	0.35	0.36	0.35	0.34	0.40	0.36	0.37	0.37	0.38	0.35	0.36	0.15	0.23
MgO	48.85	48.63	48.96	48.56	48.64	47.85	49.82	48.12	48.72	49.27	49.65	48.88	49.29	43.78	45.13
CaO	0.06	0.06	0.07	0.06	0.10	0.10	0.05	0.06	0.06	0.05	0.04	0.09	0.05	0.06	0.11
Na_2O	0.00	0.01	0.00	0.00	0.01	0.02	0.00	0.00	0.00	0.00	0.00	0.01	0.01	0.00	0.01
K_2O	0.00	0.00	0.00	0.00	0.00	0.00	0.00	0.00	0.00	0.00	0.00	0.00	0.00	0.00	0.00
Total	99.99	100.06	100.18	100.12	100.09	100.27	100.08	99.97	100.48	99.79	100.54	99.88	100.57	99.88	99.98
Fo	89.75	89.24	89.80	89.26	89.39	88.26	90.97	88.72	89.29	90.30	90.13	89.82	90.01	82.77	84.64

Table 3: Orthopyroxene major and minor element data of the studied Poiana Ruscă xenoliths. **mg#** = (Mg/(Mg + Fe)).

Sample	Ce6-8a	Ce6-10a	Ce6-11a	Ce6-16a	Ce6-16b	Ce6-17a	Ce6-17b	Ce6-18	Ce6-21	Ce6-12	Ce6-13	Ce6-2	Fi6-3	Ce6-15	Ce6-20
Type	**A**	**A**	**A**	**A**	**A**	**A**	**A**	**A**	**A**	**A**	**A**	**B**	**B**	**Fe-rich**	**Fe-rich**
(wt. %)															
SiO_2	55.04	54.52	55.15	54.60	54.67	54.82	55.64	54.56	54.67	55.32	55.41	54.33	55.93	53.12	54.62
TiO_2	0.08	0.14	0.09	0.15	0.15	0.12	0.12	0.11	0.12	0.05	0.11	0.23	0.15	0.09	0.10
Al_2O_3	4.43	4.75	3.84	4.72	4.72	4.58	3.37	4.63	4.81	3.84	4.02	4.63	3.12	4.90	3.25
Cr_2O_3	0.33	0.31	0.48	0.34	0.33	0.27	0.47	0.38	0.32	0.40	0.37	0.52	0.51	0.07	0.33
FeO	6.34	6.55	6.22	6.43	6.46	7.13	5.56	7.04	6.60	6.01	6.10	6.29	6.16	10.32	9.04
MnO	0.13	0.13	0.13	0.15	0.14	0.17	0.13	0.17	0.15	0.14	0.14	0.15	0.15	0.20	0.16
NiO	0.08	0.10	0.08	0.09	0.08	0.08	0.11	0.09	0.09	0.09	0.08	0.10	0.07	0.03	0.06
MgO	33.21	32.63	33.44	32.68	32.79	32.35	33.75	32.41	32.58	33.71	33.43	32.39	33.80	30.20	31.40
CaO	0.66	0.75	0.75	0.76	0.75	0.69	0.69	0.82	0.74	0.63	0.67	1.12	0.68	0.70	0.71
Na_2O	0.09	0.11	0.07	0.12	0.10	0.09	0.09	0.12	0.09	0.09	0.06	0.13	0.07	0.02	0.02
K_2O	0.00	0.00	0.01	0.00	0.00	0.00	0.00	0.00	0.00	0.00	0.00	0.00	0.00	0.00	0.00
Total	100.39	99.99	100.26	100.04	100.19	100.30	99.93	100.33	100.17	100.28	100.39	99.89	100.64	99.65	99.69
mg#	0.90	0.90	0.91	0.90	0.90	0.89	0.92	0.89	0.90	0.91	0.91	0.90	0.91	0.84	0.86
(ppm)															
Rb	n.d.	n.d.	0.01	0.01	0.01	0.01	0.24	0.04	n.d.	n.d.	n.d.	0.01	0.02	0.04	0.04
Ba	n.d.	n.d.	0.07	n.d.	n.d.	n.d.	0.14	n.d.	n.d.	n.d.	n.d.	n.d.	n.d.	n.d.	0.04
Th	n.d.	n.d.	n.d.	n.d.	n.d.	n.d.	n.d.	n.d.	n.d.	0.01	n.d.	n.d.	n.d.	n.d.	n.d.
U	n.d.	n.d.	n.d.	n.d.	n.d.	n.d.	n.d.	n.d.	n.d.	n.d.	n.d.	n.d.	n.d.	n.d.	n.d.
Nb	n.d.	n.d.	n.d.	0.01	0.01	n.d.	0.02	0.01	n.d.	0.01	0.01	0.05	0.01	n.d.	0.01
Ta	n.d.	n.d.	n.d.	n.d.	n.d.	n.d.	n.d.	n.d.	n.d.	n.d.	n.d.	0.01	n.d.	n.d.	n.d.
La	n.d.	n.d.	n.d.	0.01	0.01	n.d.	n.d.	n.d.	n.d.	0.01	0.01	0.02	0.01	n.d.	n.d.
Ce	n.d.	0.01	0.01	0.02	0.03	0.02	0.01	0.01	0.01	0.02	0.04	0.12	0.03	n.d.	0.01
Pb	n.d.	n.d.	n.d.	n.d.	n.d.	n.d.	n.d.	n.d.	n.d.	n.d.	n.d.	n.d.	n.d.	n.d.	n.d.
Sr	0.05	0.12	0.20	0.25	0.35	0.21	0.13	0.09	0.10	0.07	0.17	0.57	0.16	0.08	0.14
Nd	n.d.	n.d.	0.04	n.d.	0.04	n.d.	n.d.	n.d.	n.d.	n.d.	n.d.	0.12	0.06	n.d.	n.d.
Zr	0.53	1.52	0.96	1.88	1.76	1.45	1.04	0.97	1.48	0.47	1.00	3.04	0.65	0.65	0.65
Hf	0.02	0.05	0.03	0.07	0.05	0.07	0.05	0.04	0.04	n.d.	n.d.	0.09	n.d.	0.03	0.04
Sm	n.d.	0.02	n.d.	0.03	0.03	0.03	0.05	n.d.	n.d.	n.d.	n.d.	0.06	0.02	n.d.	n.d.
Eu	0.01	0.01	0.01	0.01	0.01	0.01	0.01	0.01	0.01	n.d.	0.01	0.03	0.01	0.01	n.d.
Gd	0.04	0.07	n.d.	0.06	0.06	0.05	0.04	0.04	0.04	0.03	0.04	0.08	0.03	0.04	0.04
Tb	0.01	0.01	0.01	0.01	0.01	0.01	0.01	0.01	0.01	0.01	0.01	0.02	0.01	0.01	0.00
Dy	0.08	0.13	0.09	0.14	0.13	0.13	0.08	0.11	0.10	0.07	0.10	0.15	0.08	0.08	0.08
Y	0.81	1.05	0.78	1.11	0.99	1.08	0.66	0.94	0.92	0.53	0.87	0.90	0.57	0.65	0.48
Ho	0.03	0.04	0.03	0.04	0.03	0.04	0.02	0.03	0.03	0.02	0.03	0.03	0.02	0.02	0.02
Er	0.12	0.14	0.09	0.18	0.13	0.15	0.08	0.13	0.17	0.09	0.12	0.10	0.08	0.10	0.06
Tm	0.02	0.03	0.02	0.03	0.03	0.03	0.02	0.03	0.02	0.01	0.02	0.02	0.01	0.02	0.01
Yb	0.21	0.27	0.20	0.21	0.26	0.26	0.14	0.24	0.24	0.15	0.23	0.15	0.10	0.16	0.12
Lu	0.04	0.05	0.03	0.05	0.04	0.05	0.02	0.04	0.04	0.03	0.04	0.03	0.02	0.03	0.02

(mostly olivines) (Fig. 3f). This feature suggests the development of the poikilitic texture following the above described porphyroclastic-equigranular texture. Spinel has various grain sizes and shapes. It occurs either as small, rounded grains in triple junctions or as inclusion in silicates or as large vermicular grains at curvilinear connections among silicates (Fig. 3g). In some cases small spinel grains also show a linear arrangement. In a few poikilitic samples multiphase sulphide inclusions of approximately 50–300 μm in diameter also occur (Fig. 3h). They have spheroidal, blebby or amoeboid shapes and are mostly situated in fractures of orthopyroxenes or in the spaces between spinel and orthopyroxene. The poikilitic samples show no signs of deformation or strain. Petrographic character and modal composition are rather connected: porphyroclastic-equigranular textured xenoliths have a modal olivine content >70 vol. %, whereas poikilitic texture is characteristic of samples with generally lower modal olivine content (Fig. 2 and Table 1). In correlation with the decreasing olivine content, the xenoliths become richer in orthopyroxene, generally its modes are >20 vol. %. In contrast, clinopyroxene content, apart from some xenoliths, remains constant (approximately 15 vol. %) with the increase in orthopyroxene abundance in the poikilitic series. This feature indicates that the development of the poikilitic texture was accompanied by orthopyroxene growth at the expense of olivine.

The entire series is generally poor in fluid and/or melt inclusions. However, several fluid and/or melt inclusion trails are observed, the inclusions are generally <2 μm and their linear arrangement close to grain edges and in connection with intergranular spaces suggests their secondary origin, therefore we did not take into consideration further studies of these inclusions.

Mineral chemistry

Mineral chemistry data are presented in Tables 2, 3, 4 and 5, and Figs. 4, 5 and 6. Most of the xenoliths have a very similar mineral chemistry and trace element composition with little variation. They are interpreted in this study as representing the common mantle variation beneath the studied area and are referred to in this paper as Type A xenoliths. A small number of samples, however, differ from these, especially in trace element composition and are referred to as Type B and Fe-rich xenoliths in this paper. Some clinopyroxene megacrysts were also found and analysed for comparison.

This grouping was developed especially based on trace element compositions of pyroxenes. As similar data are missing in previous studies from the same area direct comparison with those (Downes et al. 1995; Tschegg et al. 2010) is not possible. Type A xenoliths are rather homogeneous in their mineral compositions. Olivine shows a restricted composition with mg# of 88.3–89.8, NiO from 0.34 to 0.39 wt. % and CaO between 0.04 and 0.10 wt. %. The Mg-value of orthopyroxenes is somewhat higher than that of coexisting olivines with values in the range 89.0–90.3. Their Al_2O_3 contents is high, ranging from 3.37 to 4.81 wt. %, whereas CaO is low (0.66–0.82 wt. %). The most intrinsic feature of clinopyroxene compositions is high values of Al_2O_3 (5.30–7.64 wt. %) and Na_2O (1.49–1.93 wt. %). Spinel is rather homogeneous within the xenoliths and shows low cr#s of 9–18. For comparison, the xenoliths from the same area previously studied by Downes et al. (1995), are also shown on the figures. Many of them, mainly clinopyroxene-poor lherzolites, fit the Type A xenoliths' trends rather well (Tables 3 and 4, Fig. 4).

Two xenoliths (Ce6-2 and Fi6-3 lherzolites), referred to as Type B xenoliths, are slightly separate from the main chemical trends (Table 2, Fig. 4). Orthopyroxene has various Al_2O_3 contents from 3.12 to 4.63 wt. % and CaO from 0.68 to 1.12 wt. %. Clinopyroxenes have lower Al_2O_3 (4.71–5.43 wt. %) and Na_2O (1.19–1.36 wt. %) than the Type A xenoliths. Their spinels are distinct because of the elevated Cr_2O_3 (25.07–27.01 wt. %) and lower Al_2O_3 (12.63–40.95 wt. %) content, thus having the highest cr# (30.67–57.11) in the series. Ce6-2 lherzolite also shows high FeO (41.10 wt. %) and low MgO (8.60 wt. %) in spinel (Table 5). About half of the xenoliths described by Downes et al. (1995) are similar to our Type B group and differ in composition from the Type A samples, as showed for comparison on Fig. 4a–d.

The compositions of two xenoliths (Ce6-15 and Ce6-20), referred to as Fe-rich xenoliths, differ significantly from the Type A and B xenoliths. Xenolith Ce6-15 is a dunite, whereas the Ce6-20 sample has a lherzolite modal composition and very similar in mineral composition to the Ce6-15 dunite and to the pyroxenite sample analysed by Downes et al. (1995). Similar Fe-rich dunites were also reported from E-Serbia (Cvetković et al. 2010). These samples are displaced from the main residual trend (OSMA) of mantle xenoliths (Fig. 4a) and show notably lower mg# in mantle silicates (ol: 82.7–84.6; cpx: 85.3–87.9; opx: 83.9–86.0, respectively). NiO in olivine is low (0.15–0.23 wt. %), their pyroxenes have low Na_2O (cpx: 0.10–0.52 wt. %; opx: 0.41–0.51 wt. %), but relatively high Al_2O_3 (cpx: 3.84–5.60 wt. %; opx: 3.25–4.90 wt. %) and CaO (cpx~22.2 wt. %; opx: 0.70 wt. %). Their spinel composition varies over a wide range (cr#=2–21) (Table 5).

Two clinopyroxene megacrysts are uniform in composition with low mg# (83.2–83.4) and Cr_2O_3 content (0.20 wt. %) and high Al_2O_3 (8.50 wt. %) and TiO_2 (1.45 wt. %).

The mineral chemistry of xenolith samples analysed by Tschegg et al. (2010) is also shown for comparison (Fig. 4a–d). They are similar in composition to the Type A xenoliths, showing high Al and Na in pyroxenes and spinel with low cr#.

Trace element chemistry of clinopyroxenes

The trace element composition of clinopyroxenes together with their mineral chemistry is the basis of the classification of the xenoliths in this study. A great number of the xenoliths (Type A) show similar trace element concentrations (Table 4, Fig. 5). Clinopyroxenes in Type A xenoliths have a REY (rare earth elements+Y) content approx. 10×C1 chondrite, showing rather flat patterns, apart from the LREEs (light rare earth elements) which are slightly depleted with low $(La/Lu)_N$=0.2–0.5 (Fig. 5a). The REY profiles of Type B xenoliths are different with steeply downward patterns, with HREE (heavy rare earth elements) concentrations below 10×C1 chondrite and with notable LREE enrichment ($(La/Lu)_N$=2.2–4.3) (Fig. 5c). The Fe-rich xenoliths show a

Table 4: Clinopyroxene major and minor element data of the studied Poiana Ruscă xenoliths. **mg#** = (Mg/(Mg + Fe)), **Ce6-17a*** — clinopyroxene inclusion in orthopyroxene porphyroclast.

Sample	Ce6-8a	Ce6-10a	Ce6-11a	Ce6-16a	Ce6-16b	Ce6-17a	Ce6-17b	Ce6-18	Ce6-21	Ce6-12	Ce6-13	Ce6-2	Fi6-3	Ce6-15	Ce6-20	Ce6-7	Ce6-11a	Ce6-17a*
Type	**A**	**A**	**A**	**A**	**A**	**A**	**A**	**A**	**A**	**A**	**A**	**B**	**B**	**Fe-rich**	**Fe-rich**	**Megacr**	**Megacr**	
(wt. %)																		
SiO_2	51.85	51.22	51.79	51.43	51.52	51.31	52.20	51.81	51.21	51.82	51.64	51.64	52.65	50.35	51.58	48.21	48.31	
TiO_2	0.45	0.68	0.46	0.68	0.66	0.73	0.45	0.34	0.53	0.28	0.61	0.54	0.52	0.42	0.31	1.45	1.43	
Al_2O_3	6.52	7.64	6.55	7.47	7.34	7.37	5.30	6.37	7.13	6.04	6.17	5.43	4.71	5.60	3.84	8.56	8.50	
Cr_2O_3	0.70	0.72	1.25	0.85	0.76	0.66	1.29	0.77	0.67	1.02	0.92	1.15	1.16	0.10	0.52	0.20	0.21	
FeO	2.61	2.98	2.85	2.87	2.85	2.94	2.38	3.28	3.01	2.54	2.61	3.36	2.56	4.75	3.93	5.01	4.95	
MnO	0.08	0.11	0.11	0.10	0.10	0.10	0.09	0.08	0.10	0.09	0.08	0.09	0.11	0.12	0.08	0.10	0.09	
NiO	0.06	0.04	0.05	0.06	0.05	0.04	0.04	0.03	0.03	0.05	0.05	0.04	0.04	0.02	0.03	0.02	0.02	
MgO	15.38	14.85	15.26	14.91	15.08	14.83	15.97	15.46	15.27	15.55	15.40	16.63	16.18	15.46	16.11	13.98	14.02	
CaO	20.65	19.47	19.88	19.73	19.76	20.20	20.65	20.16	20.35	20.67	20.93	19.24	21.13	22.24	22.15	20.78	20.71	
Na_2O	1.61	1.93	1.79	1.89	1.86	1.77	1.49	1.65	1.50	1.46	1.48	1.36	1.19	0.41	0.51	1.09	1.11	
K_2O	0.01	0.00	0.00	0.00	0.00	0.00	0.00	0.01	0.00	0.00	0.00	0.00	0.01	0.01	0.00	0.00	0.00	
Total	99.92	99.64	99.99	99.99	99.98	99.95	99.86	99.96	99.80	99.52	99.89	99.48	100.26	99.48	99.06	99.40	99.35	
mg#	0.91	0.90	0.91	0.90	0.90	0.90	0.92	0.89	0.90	0.92	0.91	0.90	0.92	0.85	0.88	0.83	0.83	
(ppm)																		
Rb	0.18	0.01	0.59	0.93	0.01	0.04	0.23	0.20	0.08	0.05	n.d.	0.01	0.24	0.03	0.01	0.28	n.d.	0.12
Ba	0.09	n.d.	0.36	0.06	n.d.	0.12	0.10	0.13	0.05	0.11	0.09	0.05	0.16	0.09	0.05	0.77	0.08	0.03
Th	0.01	0.01	0.02	0.03	0.03	n.d.	0.29	0.12	0.01	0.82	0.24	0.21	0.02	0.02	0.03	0.07	0.06	n.d.
U	0.01	0.01	0.01	0.01	0.01	n.d.	0.13	0.04	0.01	0.18	0.10	0.05	0.02	0.01	0.01	0.01	0.01	0.01
Nb	0.01	0.07	0.27	0.33	0.30	0.01	0.22	0.08	0.04	0.22	0.44	0.79	0.14	0.01	0.01	0.87	0.61	0.01
Ta	n.d.	0.01	0.03	0.01	0.01	n.d.	0.02	0.01	0.01	0.01	0.09	0.13	0.02	0.01	n.d.	0.14	0.12	0.01
La	0.09	0.86	1.38	1.24	1.23	0.59	0.89	0.91	1.07	3.97	3.02	6.13	3.00	0.46	0.92	3.08	2.78	0.54
Ce	0.91	3.87	5.17	4.72	4.84	2.87	3.47	2.65	4.21	6.91	8.96	18.27	13.47	2.44	4.24	11.07	10.10	2.76
Pb	0.02	0.05	0.17	n.d.	n.d.	0.02	0.08	0.06	0.07	0.15	0.06	0.08	0.08	0.06	0.13	0.05	0.05	n.d.
Sr	22.33	81.97	66.38	81.65	82.14	53.53	74.53	37.53	64.88	82.97	79.43	142.00	128.86	30.05	77.26	93.13	90.30	43.00
Nd	2.08	4.49	4.76	4.96	4.96	3.81	4.56	2.66	4.48	2.55	7.71	12.23	7.47	3.58	5.08	9.81	9.32	3.75
Zr	12.45	31.33	23.90	35.50	35.44	27.52	27.92	19.13	33.06	11.32	24.70	38.17	16.37	7.54	9.57	36.63	33.10	29.80
Hf	0.58	1.02	0.69	1.07	1.04	1.02	0.89	0.60	1.03	0.44	0.66	1.21	0.52	0.39	0.46	1.73	1.46	1.12
Sm	1.24	1.80	1.57	1.82	1.87	1.66	1.71	1.19	1.80	0.85	2.41	3.13	1.75	1.44	1.67	3.01	2.60	1.76
Eu	0.54	0.76	0.69	0.78	0.76	0.74	0.67	0.50	0.71	0.39	0.88	1.06	0.62	0.50	0.54	1.06	0.97	0.74
Gd	2.05	2.61	2.09	2.65	2.55	2.44	2.15	1.87	2.49	1.35	2.76	2.98	1.89	1.65	1.66	3.08	2.86	2.63
Tb	0.38	0.45	0.37	0.47	0.46	0.46	0.36	0.37	0.47	0.25	0.44	0.41	0.29	0.26	0.23	0.42	0.39	0.49
Dy	2.93	3.36	2.66	3.42	3.32	3.35	2.45	2.78	3.36	1.90	3.14	2.47	1.89	1.67	1.44	2.57	2.39	3.65
Y	16.37	18.19	14.40	18.25	17.58	18.50	12.63	16.02	18.18	11.18	16.80	10.97	9.53	8.03	6.23	10.93	10.18	20.13
Ho	0.64	0.72	0.57	0.72	0.69	0.72	0.48	0.62	0.71	0.42	0.65	0.44	0.37	0.33	0.26	0.44	0.41	0.79
Er	1.89	2.00	1.60	2.06	1.99	2.02	1.36	1.83	2.08	1.28	1.90	1.06	1.02	0.87	0.66	1.08	0.99	2.27
Yb	1.86	2.01	1.52	1.94	1.90	2.06	1.15	1.89	2.07	1.26	1.74	0.93	0.97	0.79	0.59	0.78	0.73	2.29
Lu	0.26	0.27	0.21	0.28	0.26	0.28	0.16	0.26	0.27	0.18	0.25	0.12	0.14	0.10	0.08	0.10	0.09	0.32
Sc	62.97	59.80	60.30	54.38	56.90	62.44	64.82	58.45	58.12	66.84	63.42	51.47	66.37	52.36	61.53	57.20	53.30	59.70
V	301.33	272.30	281.80	260.11	296.00	310.27	270.67	263.17	288.80	272.33	297.33	262.33	293.17	252.00	250.71	352.67	329.50	293.00
Cr	6090.0	4737.0	9368.0	5557.8	6186.0	5245.5	9755.0	6245.0	5314.0	7337.8	6598.3	8083.3	8961.7	791.3	4408.6	883.00	1475.0	5490.0
Co	22.97	24.70	22.00	27.09	23.94	23.70	21.92	23.98	23.32	21.84	22.02	25.46	22.70	32.04	31.47	31.47	29.10	23.55
Ni	368.67	308.20	349.20	396.56	383.60	345.18	373.67	362.83	362.80	363.11	345.50	366.00	368.17	175.08	279.00	173.33	175.50	343.50
La/Lu(N)	0.04	0.33	0.69	0.46	0.49	0.22	0.59	0.37	0.41	2.24	1.27	4.37	2.28	0.47	1.24	3.12	3.19	0.17

Table 5: Spinel major element data of the studied Poiana Ruscă xenoliths. **mg#** = (Mg/(Mg + Fe)), **cr#** = (Cr/(Cr + Al)).

Sample	Ce6-8a	Ce6-10a	Ce6-11a	Ce6-16a	Ce6-16b	Ce6-17a	Ce6-17b	Ce6-18	Ce6-21	Ce6-12	Ce6-13	Ce6-2	Fi6-3	Ce6-15	Ce6-20
Type	**A**	**A**	**A**	**A**	**A**	**A**	**A**	**A**	**A**	**A**	**A**	**B**	**B**	**Fe-rich**	**Fe-rich**
(wt. %)															
SiO_2	0.03	0.03	0.03	0.06	0.03	0.03	0.05	0.08	0.04	0.02	0.02	0.03	0.04	0.04	0.04
TiO_2	0.07	0.13	0.12	0.13	0.13	0.11	0.16	0.07	0.10	0.05	0.15	9.80	0.36	0.13	0.51
Al_2O_3	56.94	58.07	50.29	57.52	58.27	59.36	46.98	54.05	57.92	52.78	55.67	12.63	40.95	60.06	43.91
Cr_2O_3	10.26	8.28	16.70	9.81	9.05	7.75	20.85	11.26	8.67	15.02	11.92	25.07	27.01	2.10	18.06
FeO	10.75	11.61	12.38	10.47	10.56	11.18	11.60	12.75	11.29	11.16	10.61	41.10	13.11	18.06	20.72
MnO	0.09	0.11	0.10	0.13	0.11	0.11	0.15	0.15	0.14	0.09	0.12	0.46	0.16	0.11	0.18
NiO	0.34	0.36	0.33	0.33	0.19	0.33	0.26	0.46	0.41	0.31	0.34	0.27	0.21	0.21	0.25
MgO	21.10	21.40	19.50	20.63	20.91	20.91	19.60	20.57	20.81	20.25	20.91	8.66	17.99	18.41	15.84
CaO	0.00	0.00	0.00	0.00	0.01	0.00	0.00	0.00	0.00	0.00	0.00	0.01	0.00	0.00	0.00
Na_2O	0.00	0.00	0.00	0.00	0.01	0.00	0.00	0.06	0.00	0.00	0.00	0.00	0.00	0.00	0.00
K_2O	0.00	0.00	0.00	0.00	0.00	0.00	0.00	0.00	0.00	0.00	0.00	0.00	0.00	0.00	0.00
Total	99.58	99.99	99.45	99.08	99.27	99.78	99.65	99.44	99.38	99.68	99.74	98.03	99.83	99.12	99.51
mg#	0.78	0.77	0.74	0.78	0.78	0.77	0.75	0.74	0.77	0.76	0.78	0.27	0.71	0.65	0.58
cr#	0.11	0.09	0.18	0.10	0.09	0.08	0.23	0.12	0.09	0.16	0.13	0.57	0.31	0.02	0.22

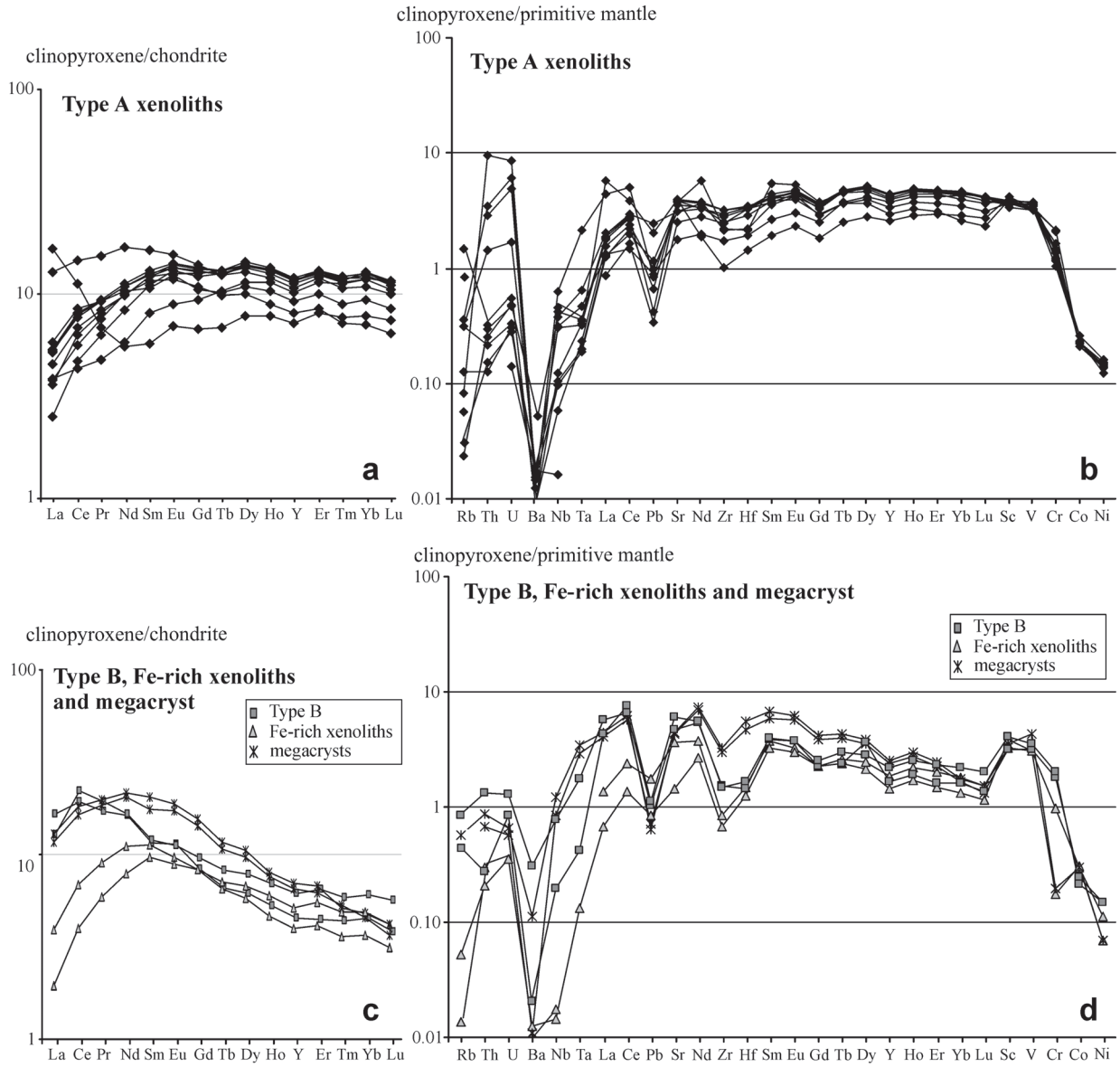

Fig. 5. C1 chondrite normalized (data from McDonough & Sun 1995) REY patterns and PM-normalized (Sun & McDonough 1989) trace element patterns of clinopyroxenes.

convex-upward REY shape with both LREE and HREE-depletion and a maximum at Sm. The Ce6-20 lherzolite has high $(La/Lu)_N = 1.2$, whereas the Ce6-15 dunite has a ratio similar to the Type A samples (0.5). Clinopyroxene megacrysts have REY patterns roughly similar to Fe-rich xenoliths, however they are enriched in LREEs and have a high $(La/Lu)_N$ ratio (ca. 3.1). The patterns have steeply downward shapes with maxima at Nd coupled with a slight LREE depletion.

Total REE concentrations in clinopyroxenes are generally low (Type A: 32–50 ppm; Type B: 37–42 ppm), except for the Fe-rich xenoliths, which have even lower total REE concentrations (22–24 ppm). Megacrysts have slightly higher REE_{tot} concentrations (44–47 ppm).

Extended multi-element patterns of clinopyroxenes in all types of xenoliths are roughly similar (Fig. 5b) with a notable (Ba-)Nb(-Ta) negative anomaly and sometimes a Th-U trough. Type B and Fe-rich xenoliths also have pronounced Zr-Hf negative anomalies. All xenoliths exhibit a Pb negative anomaly. Megacrysts have a slightly different extended multi-element pattern, lacking a Nb-Ta anomaly and steeply downward shape for the HREEs.

Trace element chemistry of orthopyroxenes

Orthopyroxenes from Poiana Ruscă xenoliths have very low REE contents (0.01–1×C1 chondrite) (Fig. 6). Patterns of all types are rather similar to each other and exhibit a continuous depletion from HREE to LREE ($(La/Lu)_N = 0.01–0.03$).

Discussion

Main physical and chemical characteristics of the lithospheric mantle beneath the Poiana Ruscă

Type A xenoliths form the most abundant lithology, hence the main mantle processes and mineralogy will be discussed based on them in the following. The Type A xenolith series shows a significant variation in both modal composition and texture (Table 1, Fig. 2). However, the chemical composition of these xenoliths follows a single chemical trend. Therefore, the mantle portion, represented by these xenoliths, regardless of the textural variation, was equilibrated in a relatively narrow T range between 930 and 1020 °C (Table 1). The Poiana Ruscă Type A xenoliths sampled a weakly depleted mantle segment, which experienced only a low degree (< 10 %) of basaltic melt removal, according to the low cr# (8–23) of spinel and calculations (Hellebrand et al. 2001), based on the spinel Cr-number (Table 2). The olivine-spinel mantle array "OSMA" (Fig. 4a) and $Y_{(N)}$–$Yb_{(N)}$ diagram (Fig. 7) also show that the Type A xenoliths fall within the field of common mantle (Arai 1994) and experienced only a low degree of melting. Based on the fractional melting model with Y and Yb contents in clinopyroxenes (Fig. 7), proposed by Norman (1998), this depletion is <8 %. High Al- and Na-content and the general low mg# of the pyroxenes (Fig. 4b,c,d) are also in agreement with slightly different but generally low degrees of mafic melt extraction.

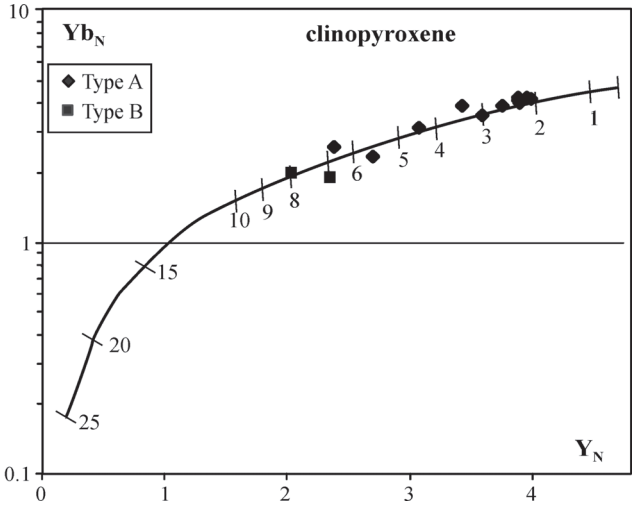

Fig. 7. Y_N vs. Yb_N ratios of clinopyroxenes in Type A and Type B xenoliths with the fractional melting model proposed by Norman (1998).

The Type B xenoliths differ from the Type A ones in their more depleted character, showing the highest degree of partial melting in the series (Figs. 4a, 7), the highest olivine content (Table 1) and also their spinel are the richest in chromium (cr# 30–57) (Table 5). Nevertheless, the Type B xenoliths have clinopyroxene with lower Al- and Na-contents and more enriched REY patterns than the Type A xenoliths (Fig. 5) and show the highest equilibrium temperature (980–1110 °C). This all indicates that the lithospheric mantle represented by the Type B xenoliths could have undergone a higher degree of partial melting, and subsequently experienced small scale metasomatism.

Most Poiana Ruscă xenoliths from the Cerbal and Panc localities, previously studied by Downes et al. (1995), fit the studied Type A xenoliths' trends well (Fig. 4a–d). About half of their studied xenoliths,

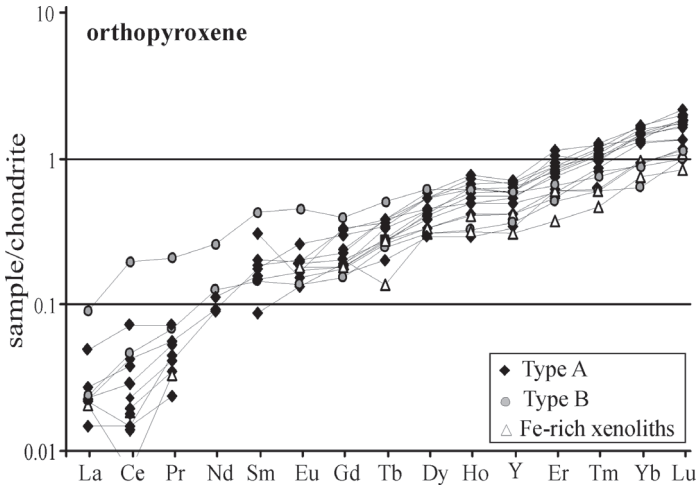

Fig. 6. C1 chondrite normalized (data from McDonough & Sun 1995) REY patterns of orthopyroxenes.

however, are detached from the principal group, and resemble the Type B xenoliths (Fig. 4a–d). Therefore, we cannot exclude the possibility that these more depleted and subsequently refertilized xenoliths are more common in the mantle beneath the Poiana Ruscă Mts, but only poorly sampled in our series. This is also supported by Cvetković et al. (2004) who described an extremely depleted mantle in the very vicinity of the studied area, underneath East Serbia. One pyroxenite, described by Downes et al. (1995), is similar to the studied Fe-rich xenoliths. Because Downes et al. (1995) did not study trace element distributions, any further comparison with their samples is rather difficult.

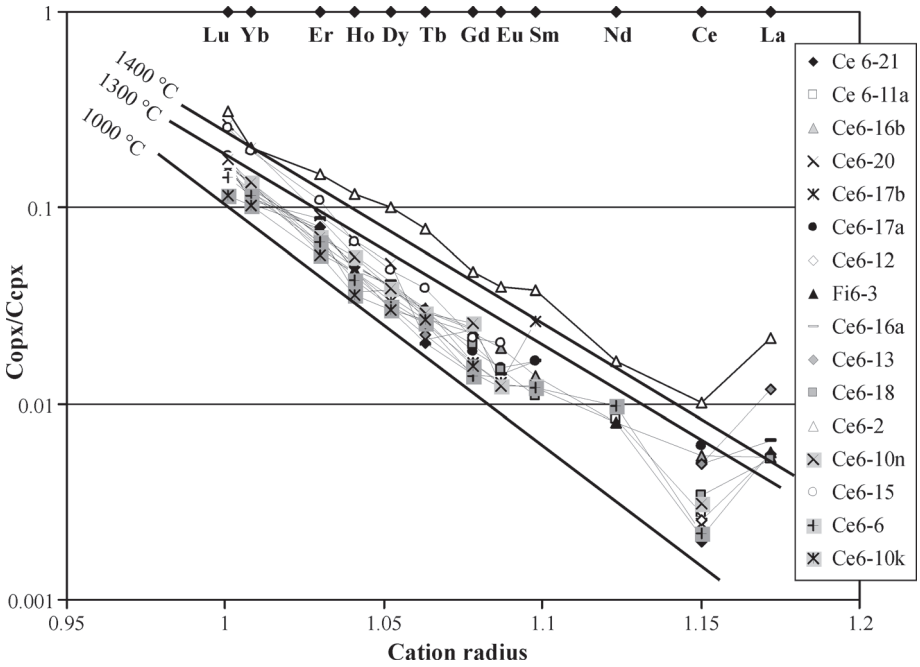

Fig. 8. Partitioning of the rare earth elements between orthopyroxene/clinopyroxene as a function of cation radius. Equilibrium lines for three different temperatures after (Agranier & Lee 2007).

Recently Tshegg et al. (2010) studied 6 xenoliths from Cerbal and 1 xenolith from Stancesti in Poiana Ruscă (Fig. 1). They observed a general occurrence of reaction coronas around ortho- and clinopyroxenes and interpreted them as interaction products between mantle minerals and infiltrated host mafic melt. In fact, they described the xenoliths as "thermally affected by the host magmas". For these reasons and because we are unable to examine and exclude the effects of any possible chemical modification of the xenoliths by host melt infiltration and/or thermal effects, we prefer not to use these data systematically for comparison in our present paper.

The mostly anhydrous character of the mantle can be deduced from the absence of OH-bearing minerals in agreement with Downes et al. (1995) who also found no hydrous minerals in their suite of xenoliths either. The complete absence of primary fluid and silicate melt inclusions in the studied xenolith samples also supports this character.

Evaluation of the possible contamination of the xenoliths by the host melt

Because of the small dimensions of the xenoliths, it is possible that the chemistry of the smallest xenoliths was modified by host mafic magma contamination or by recent metasomatism by the pre-eruptive magmatic precursor processes (e.g. Stosch 1982; Zindler & Jagoutz 1988; Witt-Eickschen & O'Neill 2005). To avoid utilizing contaminated xenoliths for the characterization of pervasive geochemical mantle features beneath Poiana Ruscă, we investigated the possibility of contamination for each xenolith studied. The distribution of REE between minerals (for example, orthopyroxene–clinopyroxene or olivine–orthopyroxene (Agranier & Lee 2007)) clearly shows whether the xenoliths escaped or went through recent chemical modifications. To test the chemical equilibrium/disequilibrium state of the xenoliths, the equilibrium partitioning of the REE between clinopyroxene and orthopyroxene of each xenolith was calculated. At chemical equilibrium there is a negative correlation between ratios of REE abundances of orthopyroxene/clinopyroxene when plotted as a function of cation radii and any deviations from this equilibrium can be considered as a recent metasomatism/contamination (Agranier & Lee 2007). Orthopyroxene/clinopyroxene REE ratios show a very monotonous negative correlation of the cation ratio for each xenolith of the studied suite (Fig. 8), nearly parallel to the distribution trend, or more precisely to the equilibrium partitioning model, developed for different temperatures by Agranier & Lee (2007). For our studied xenoliths, the only deviation from the equilibrium trends is in La (Fig. 8). This indicates that the xenoliths could have suffered some recent contamination by the host magma, but this enrichment affected only the most incompatible elements and most of the REE abundances reflect the primary characteristics of the mantle from which the xenoliths were derived.

Only a few xenoliths deviate notably from the equilibrium distribution (Fig. 8), suggesting different degrees of recent contamination and therefore their chemistry probably does not represent primary mantle characteristics. Among these deviating xenoliths, the Type B Ce6-2 lherzolite is identical in its REY pattern to the host mafic melt (Fig. 9), although it must have been in equilibrium with the melt calculated. However, because of its very small dimensions (1–2 cm in diameter) it was probably significantly contaminated by the host basanite. Type A Ce6-17b lherzolite also shows some deviation in the LREE from the equilibrium lines (Fig. 8), which supports a slight degree of recent contamination from the host magma. These samples are excluded from further interpretation.

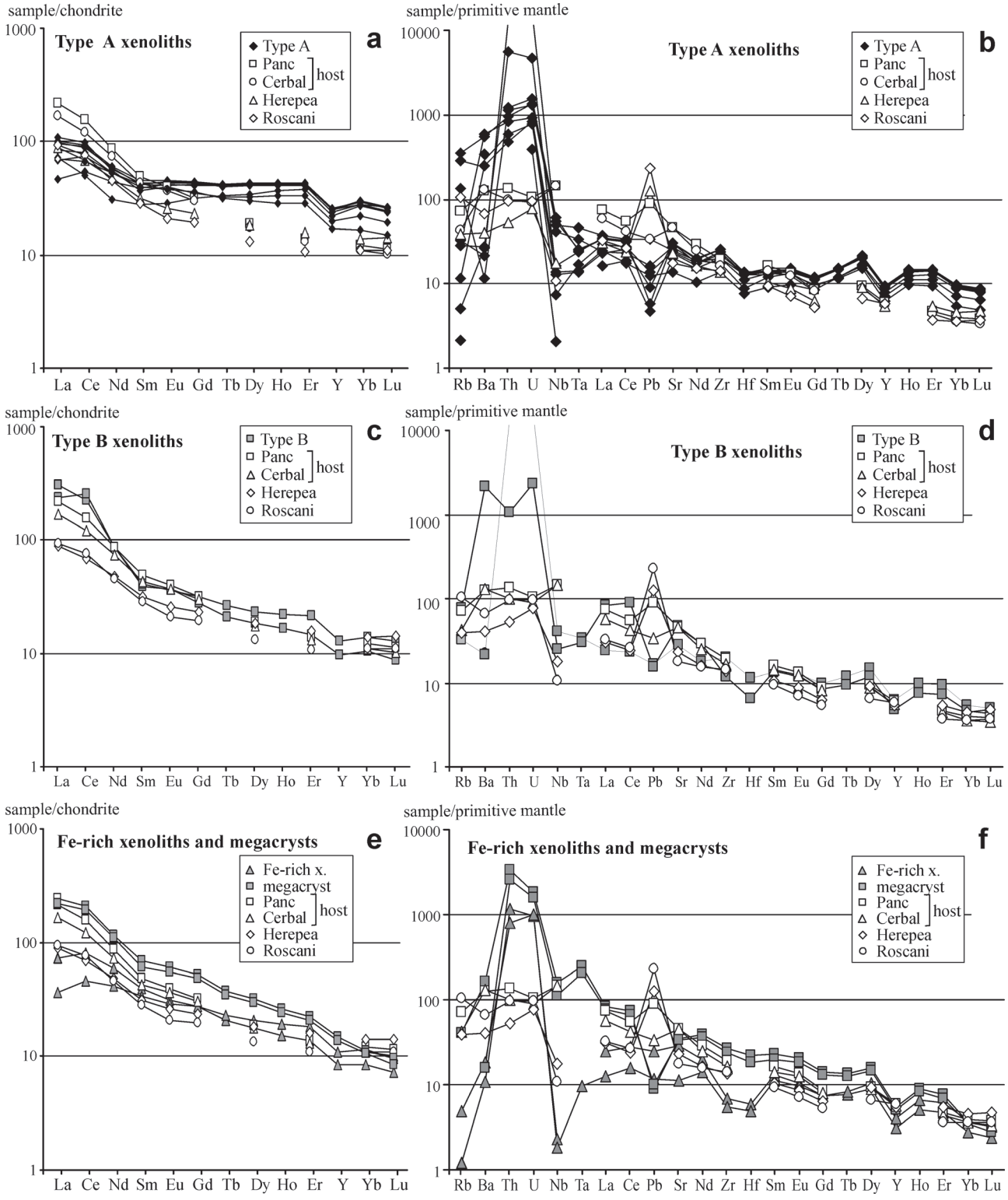

Fig. 9. Calculated melt composition in equilibrium with the clinopyroxenes (partition coefficients for Ba, Nb, La, Ce, Pb, Sr, Nd, Zr, Y, Yb, Lu after Hart & Dunn (1993), for Rb, Th, U, Eu, Gd, Tb, Dy, Ho, Er after McKenzie & O'Nions (1991) and for Ta after Green et al. (2000).

Origin of Fe-rich xenoliths and megacrysts

The Ce6-15 Fe-dunite and Ce6-20 Fe-lherzolite samples differ significantly from the other xenoliths in their modal composition (high olivine and relatively low orthopyroxene content) (Table 1), Fe-rich character of pyroxenes, LREE and HREE-depleted REY patterns of clinopyroxene (Fig. 5c,d, Table 4) and lower equilibrium temperature (ap-

proximately 900 °C), suggesting a different origin. The REY patterns of melts in equilibrium with xenolith clinopyroxenes were calculated (see details of calculation in the next section). The trace element patterns of the calculated melt composition are different from those of the Type A and B xenoliths, showing less LREE-enrichment and slightly decreasing REY patterns (Fig. 9a,c). Comparing the REY patterns of melts in equilibrium with clinopyroxenes of Fe-rich xenoliths to the Poiana Ruscă Upper Cretaceous basaltic andesites (Downes et al. 1995) and Paleocene–Eocene host mafic rocks (Downes et al. 1995) (Fig. 9e), Fe-rich xenoliths have a REY pattern similar to the basaltic andesites. However their extended trace element pattern also shows notable differences (e.g. significant Th-U positive anomaly and depletions in HFS elements (Nb, Ta, Zr, Hf and Y) (Fig. 5c,d)).

Clinopyroxene megacrysts also show a rather different REY pattern compared to the Type A xenoliths (Fig. 5c,d, Table 4). They are more enriched in LREEs and have a steeply downward shape throughout the whole REY pattern. Moreover, they have a high Th, U and slightly low Nb, Ta concentrations (Table 4). The composition of the calculated melt in equilibrium with the megacrysts resembles the mafic host (Fig. 9), although there are some differences. For instance, the calculated melt in equilibrium with megacrysts is very rich in Th-U and richer in HREE than the host rocks, however they are very similar in their lack of a Nb negative anomaly.

This suggests that Fe-rich xenoliths and megacrysts are deep-seated crystallization products of mafic magmas, in agreement with the widespread interpretations of megacrysts and pyroxenites as direct precipitates from mafic alkaline and the Fe-dunites from high Mg-magmas (e.g. Binns et al. 1970; Wilshire & Shervais 1975; Frey & Prinz 1978; Dobosi & Jenner 1999; Cvetković et al. 2010). The Fe-rich xenoliths may have crystallized from the older basaltic andesitic magmas of Poiana Ruscă or from similar magmas and subsequently entrained by the younger host basaltic magmas. In contrast, the megacrysts are cogenetic with the host basalts.

The orthopyroxene-enrichment and poikilitic texture formation

Orthopyroxene-rich xenoliths constitute a minor part of the lithospheric mantle and may originate by distinct process(es). Such xenoliths have been interpreted as mantle residues after extensive melt extraction (Ringwood 1958), however, this seems to be unlikely for the studied xenoliths for several reasons. The petrography of the Poiana Ruscă Type A xenoliths suggests that a slightly deformed porphyroclastic-equigranular texture was overprinted by the poikilitic texture (Fig. 3b,c and e), where orthopyroxene was growing at the expense of olivine. Besides, >32 % modal orthopyroxene cannot be formed by classic partial melting models, rather they can be formed by reaction of an olivine-rich peridotite and a siliceous melt (Kelemen et al. 1998). Silicate minerals in the Poiana Ruscă xenoliths have nearly constant mg# and olivines have constant Ni contents with an increasing orthopyroxene content (Tables 1 and 2), whereas xenoliths formed by a high degree of partial melting should show a positive correlation of increasing mg# in silicates and increasing Ni in olivine with the increasing modal composition of orthopyroxene, namely an increasing degree of partial melting. Moreover, the cr# of spinels is rather low (8–23) (Table 5), indicating only a low degree (< 10 %) of melt extraction as discussed earlier.

Several studies have proposed the origin of orthopyroxene-enriched rocks via metasomatic reactions between more or less depleted lithosphere peridotite and percolating melts/fluids for lithologies in a wide range of tectonic settings from all over the world (e.g. Kelemen et al. 1992; Smith et al. 1999; McInnes et al. 2001; Santos et al. 2002; Arai et al. 2003, 2004, 2006; Bali et al. 2007, 2008; Rehfeldt et al. 2008; Dantas et al. 2009). Most studies explain orthopyroxene-enrichment of the mantle rocks either by reaction with aqueous SiO_2-rich melts derived from slab dehydration and melting (e.g. Kelemen et al. 1992; Arai et al. 2003, 2004) or by evolved, silica-saturated alkali magmas percolating through the mantle (e.g. Arai et al. 2006; Dantas et al. 2009). Some recent studies from the Carpathian-Pannonian-Balkan Region have interpreted the formation of orthopyroxene-enriched mantle lithologies as resulting from a percolating melt in the subcontinental lithosphere related to the melting of subducted slabs (Cvetković et al. 2004, 2007; Marchev et al. 2006; Bali et al. 2007, 2008; Berkesi et al. 2012) or via magmatic liquids emerging from the asthenosphere associated with lithosphere thinning (Embey-Isztin et al. 1989, 2001; Embey-Isztin & Dobosi 2011).

The petrography and chemistry of the studied poikilitic xenoliths suggest formation of orthopyroxene by reaction of slightly deformed and depleted peridotitic mantle rocks with a silicate melt. Their poikilitic texture with large orthopyroxene crystals, embedding olivines (Fig. 3b,c and e), suggests orthopyroxene growing at the expense of the other silicates, mainly olivine. The orthopyroxenes and clinopyroxenes in the studied xenoliths are very rich in Al and Na (Fig. 4, Tables 3 and 4). However, Al + Na cannot be derived from olivine, hence the percolating melt needed to be enriched in these elements. Therefore, we can suppose the modification of the mantle lithologies was by means of an Al + Na-rich silicate melt. Orthopyroxenes from the Massif Central (Xu et al. 1998), SW Japan (Arai et al. 2006) and N Patagonia (Dantas et al. 2009), with similar Al-rich compositions, were also described as resulting from a melt percolation-reaction-crystallization process in a lherzolite precursor (Xu et al. 1998) and as reaction products of highly evolved alkaline melts (Wulff-Pedersen et al. 1996, 1999; Arai et al. 2006) or alkaline-subalkaline (Dantas et al. 2009) with mantle olivine.

The pyroxenes in the whole series are poor in LREE (Type A cpx: REE total 30–45 ppm; $La/Lu_{(N)} = 0.04–0.60$) (Table 4), which can be explained by an incompatible trace element poor melt reacting with mantle rock. Because volatile-rich fluids have a great capacity to transport many incompatible elements (e.g. Manning 2004), such fluids were unlikely to have been in contact with the studied mantle segment. The very rare occurrence of fluid/melt inclusions in the studied xenoliths also confirms the volatile-poor feature of the percolating and reacting melt.

To test what melt type could have been responsible for the reaction, we calculated liquid composition in equilibrium with the clinopyroxenes using crystal/melt partition coefficients after McKenzie & O'Nions (1991), Hart & Dunn (1993) and

Green et al. (2000). The calculated melt compositions in equilibrium with the clinopyroxenes of the Type A xenoliths have roughly flat, slightly LREE-enriched and slightly HREE-depleted patterns (Fig. 9a). The calculated melts in the extended trace element diagrams show roughly similar patterns for all groups (Fig. 9b). All patterns are characterized by significant positive Th-U anomaly. Strong Pb negative anomaly (Ce/Pb = 40–170), with the exception of the Ce6-11a wehrlite, is notable suggesting that the melt was rather depleted in Pb. A slight Nb-Ta negative anomaly is also characteristic. Moreover, Zr shows a slight peak relative to the Hf. The Type B xenoliths have more LREE-enriched REY patterns than the Type A ones. Enrichments in LILE and depletions in high field strength (HFS) elements (Nb, Ta, Zr, Hf, Ti) of calculated melt composition (Fig. 9c and d) can indicate little similarity to the subduction related fluids/melts (e.g. Manning 2004).

The geochemistry of the Type A xenoliths and calculated melt composition in equilibrium with the xenolith clinopyroxenes suggests that the formation of the poikilitic texture and the orthopyroxene-enrichment of the lithospheric mantle beneath Poiana Ruscă was linked to an Al- and alkali-rich, volatile-poor mafic melt. Xenolith pyroxenes have an overall REE-poor and LREE-depleted character. A melt percolating in the mantle for a long time can react several times with the peridotitic wall rock and during these metasomatic events can lose the majority of its incompatible trace element content, while retaining its original less incompatible and compatible element content. A similar melt to the calculated melt composition in equilibrium with the Poiana Ruscă xenolith clinopyroxenes was described from N-Patagonia causing orthopyroxene-enrichment in websterite xenoliths (Dantas et al. 2009), which are identical in REY pattern to the studied Type A xenoliths (Fig. 10). Wulff-Pedersen et al. (1999) also described that the IRC-process (basaltic melt infiltration, reaction and crystallization) can form evolved Si-rich, REE-poor melts with low LREE/HREE ratios. Clinopyroxene-rich lherzolite (Cpx-L) xenoliths from East Serbia (Cvetković et al. 2004) also show similarities to the Poiana Ruscă xenoliths, however these xenoliths are more enriched in LREEs (Fig. 10).

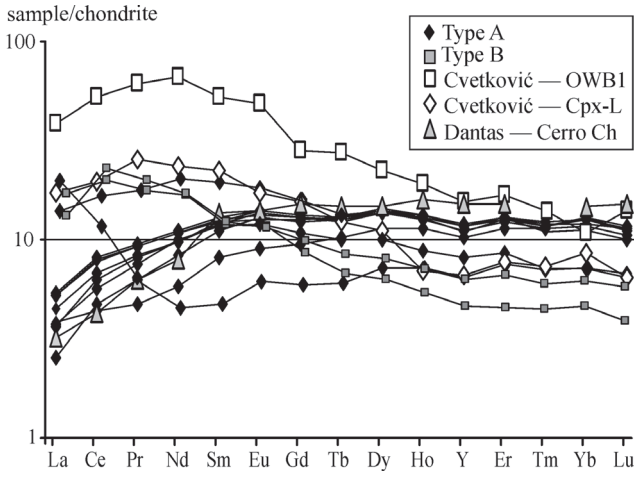

Fig. 10. Comparative REE patterns of the clinopyroxenes from orthopyroxene-enriched xenoliths from the Carpathian-Pannonian-Balkan Region (Cvetković et al. 2004) and from N-Patagonia (Dantas et al. 2009).

Geodynamic remarks

During the Late Mesozoic rifting-spreading-subduction events (e.g. Schmid et al. 2008), various melts from an originally heterogeneous mantle could have been formed within the subcontinental mantle and impregnated it beneath the studied lithospheric mantle section. Some of these melts, related to the subduction events of the Severin and/or Vardar-Axios paleo-oceans (e.g. Janković 1997; Berza et al. 1998) could have reached the mantle beneath Poiana Ruscă, after migrating for a time in the mantle. Cvetković et al. (2013) also hypothesized that the East Serbian magmatic rocks of the same age (60–70 Ma) could be the results of the magmatic activity immediately post-dating the subduction and formation of Upper Cretaceous magmatic rocks of the Banatite-Timok-Srednjegorje Belt (banatites), developed along the margin of the European plate. Deep lithospheric fractures at the boundary between the Tisza and Dacia zones could permit these small volume basaltic melts to reach the surface (Downes et al. 1995). This is in agreement with the interpretation of Tschegg et al. (2010) of the Poiana Ruscă magmatic activity being asthenospheric decompression melting. Reaction with the subduction-related early (66–72 Ma) andesitic melts of Poiana Ruscă (Herepea, Roscani) can also be a plausible explanation for the formation of the poikilitization event studied in the mantle xenoliths, considering the good agreement for LREEs with the calculated liquid composition in equilibrium with the Poiana Ruscă Type A xenoliths (Fig. 9a). However interaction with such a melt hardly justifies the difference of the calculated liquid in HREEs.

Conclusions

- Moderate-low mg# of olivines and pyroxenes and low cr# of spinel suggest that the mantle segment beneath Poiana Ruscă experienced a low degree (< 10 %) of mafic melt removal. Furthermore, the Type A xenoliths are generally poor in overall REEs and have rather flat REY patterns with slight LREE-depletion;
- The predominant lithology of the lithospheric mantle beneath Poiana Ruscă, represented by the Type A xenoliths, suggests that a slightly deformed porphyroclastic-equigranular textured series represents the early mantle characteristics, which were overprinted by orthopyroxene growth and poikilitic texture formation at the expense of olivine;
- Such geochemistry of the Type A xenoliths and calculated melt composition in equilibrium with the xenolith clinopyroxenes suggest that the percolating melt, caused formation of poikilitic texture in the mantle portion represented by the Type A xenoliths. This melt could have been a mafic, Al-Na-rich, volatile-poor melt. Little similarity is seen to the Late Cretaceous–Paleogene (66–72 Ma) subduction-related andesitic magmatism of Poiana Ruscă;

• Subsequent passage of mafic melts in the mantle, with similar compositions to the older andesitic magmatism of Poiana Ruscă, is recorded in the pyroxenites (Fe-rich xenoliths). These pyroxenites are similar to Cpx-rich lherzolites, occurring in the E Serbian rocks, whereas the megacrysts seem to be cogenetic with the host basanite.

Acknowledgments: The authors thank the members of the Lithosphere Fluid Research Lab (Eötvös University, Budapest) for constructive discussions and indispensable help in sample collection. The authors would like to thank Hilary Downes for her kind advice and useful suggestions. The reviews by Enikő Bali and Vladica Cvetković were very much appreciated for the improvement of the manuscript. Many thanks go to Géza Császár for making possible microprobe analysis, as well as to Terry Williams, Teresa Jeffries, John Pratt, Anton Kearsley, Tony Wighton (Natural History Museum, London) and Nagy Géza (Hungarian Academy of Sciences, Institute for Geological and Geochemical Research, Budapest) for technical help in microprobe and LA-ICP-MS analysis. These studies were supported by Grants from the Hungarian National Scientific Research Foundation to Zsuzsanna Nédli and Géza Császár (PF 64020 and K 62468 Projects), to Zsuzsanna Nédli for the Synthesys Project (GB-TAF 4146 Project) and to Júlia Dégi for the TéT Project. This is the 62nd publication of the Lithosphere Fluid Research Lab, Eötvös University, Budapest.

References

Agranier A. & Lee C.-T.A. 2007: Quantifying trace element disequilibria in mantle xenoliths and abyssal peridotites. *Earth Planet. Sci. Lett.* 257, 290–298.

Arai S. 1994: Characterization of spinel peridotites by olivine–spinel compositional relationships: Review and interpretation. *Chem. Geol.* 113, 191–204.

Arai S., Ishimaru S. & Okrugin V. 2003: Metasomatized harzburgite xenoliths from Avacha volcano as fragments of mantle wedge of the Kamchatka arc: implication for the metasomatic agent. *Island Arc* 12, 233–246.

Arai S., Takada S., Michibayashi M. & Kida M. 2004: Petrology of peridotite xenoliths from Iraya volcano, Philippines, and its implication for dynamic mantle-wedge processes. *J. Petrology* 45, 369–389.

Arai S., Shimizu Y., Morishita T. & Ishida Y. 2006: A new type of orthopyroxenite xenolith from Takashima, Southwest Japan: silica enrichment of the mantle by evolved alkali basalt. *Contr. Mineral. Petrology* 152, 387–398.

Bali E., Falus Gy., Szabó Cs., Peate D.W., Hidas K., Török K. & Ntaflos T. 2007: Remnants of boninitic melts in the upper mantle beneath the central Pannonian Basin? *Miner. Petrology* 90, 51–72.

Bali E., Zajacz Z., Kovács I., Szabó Cs., Halter W., Vaselli O., Török K. & Bodnar R.J. 2008: A quartz-bearing orthopyroxene-rich websterite xenolith from the Pannonian Basin, Western Hungary: Evidence for release of quartz-saturated melt from a subducted slab. *J. Petrology* 49, 421–439.

Ballhaus C., Berry R.F. & Green D.H. 1991: High pressure experimental calibration of the olivine–orthopyroxene–spinel oxygen geobarometer: implications for the oxidation state of the upper mantle. *Contr. Mineral. Petrology* 107, 27–40.

Berkesi M., Guzmics T., Szabó Cs., Dubessy J., Bodnar R.J., Hidas K. & Ratter K. 2012: The role of CO_2-rich fluids in trace element transport and metasomatism in the lithospheric mantle beneath the Central Pannonian Basin, Hungary, based on fluid inclusions in mantle xenoliths. *Earth Planet. Sci. Lett.* 331–332, 8–20.

Berza T., Constantinescu E. & Vlad S.N. 1998: Upper Cretaceous magmatic series and associated mineralisation in the Carpathian–Balkan Orogen. *Resour. Geol.* 48, 4, 281–306.

Binns R.A., Duggan M.B. & Wilkinson J.F.G. 1970: High pressure megacrysts in alkaline lavas from north-eastern New South Wales. *Amer. J. Sci.* 269, 132–168.

Brey G.P. & Köhler T.P. 1990: Geothermobarometry in four phase lherzolites. II. New thermobarometers and practical assessment of existing thermobarometers. *J. Petrology* 31, 1353–1378.

Ciobanu C., Cook N.J. & Stein H. 2002: Regional setting and geochronology of the Late Cretaceous Banatitic magmatic and metallogenetic belt. *Mineralium Depos.* 37, 541–567.

Cvetković V., Downes H., Prelević D. & Jovanović M. 2004: Characteristics of the lithospheric mantle beneath East Serbia inferred from ultramafic xenoliths in Palaeogene basanites. *Contr. Mineral. Petrology* 148, 335–357.

Cvetković V., Lazarov M., Downes H. & Prelević D. 2007: Modification of the subcontinental mantle beneath East Serbia: Evidence from orthopyroxene-rich xenoliths. *Lithos* 94, 90–110.

Cvetković V., Downes H., Hock V., Prelević D. & Lazarov M. 2010: Mafic alkaline metasomatism in the lithosphere underneath East Serbia: evidence from the study of xenoliths and the host alkali basalts. *Geol. Soc. London, Spec. Publ.* 337, 213–239.

Cvetković V., Šarić K., Prelević D., Genser J., Neubauer F., Höck V. & von Quadt A. 2013: An anorogenic pulse in a typical orogenic setting: The geochemical and geochronological record in the East Serbian latest Cretaceous to Palaeocene alkaline rocks. *Lithos* 180–181, 181–199.

Dantas C., Grégoire M., Koester E., Conceição R.V. & Rieck Jr. N. 2009: The lherzolite–websterite xenolith suite from Northern Patagonia (Argentina): Evidence of mantle-melt reaction processes. *Lithos* 107, 107–120.

Dobosi G. & Jenner G.J. 1999: Petrologic implications of trace element variation in clinopyroxene megacrysts from the Nógrád volcanic province, north Hungary: a study by laser ablation microprobe-inductively coupled plasma-mass spectrometry. *Lithos* 46, 731–749.

Downes H. 2001: Formation and modification of the shallow subcontinental lithospheric mantle: a review of geochemical evidence from ultramafic xenolith suites and tectonically emplaced ultramafic massifs of Western and Central Europe. *J. Petrology* 42, 233–250.

Downes H., Vaselli O., Seghedi I., Ingram G., Rex D., Coradossi N., Pécskay Z. & Pinarelli L. 1995: Geochemistry of late Cretaceous–early Tertiary magmatism in Poiana Ruscă (Romania). *Acta Vulcanol.* 7, 209–217.

Embey-Isztin A. & Dobosi G. 2011: The origin and significance of poikilitic and mosaic peridotite xenoliths in the western Pannonian Basin. *Bull. Hung. Geol. Soc.* 141, 267–281 (in Hungarian).

Embey-Isztin A., Scharbert H.G., Dietrich H. & Poulditis H. 1989: Petrology and geochemistry of peridotite xenoliths in alkali basalts from the Transdanubian Volcanic Region. *J. Petrology* 34, 317–343.

Embey-Isztin A., Dobosi G., Altherr R. & Meyer H.P. 2001: Thermal evolution of the lithosphere beneath the western Pannonian Basin: evidence from deep-seated xenoliths. *Tectonophysics* 331, 285–306.

Frey F.A. & Prinz M. 1978: Ultramafic inclusions from San Carlos, Arizona: petrologic and geochemical data bearing on their petrogenesis. *Earth Planet. Sci. Lett.* 38, 129–176.

Green T., Blundy J., Adam J. & Yaxley G. 2000: SIMS determina-

tion of trace element partition coefficients between garnet, clinopyroxene and hydrous basaltic liquids at 2–7.5 GPa and 1080–1200 °C. *Lithos* 53, 165–187.

Hart S.R. & Dunn T. 1993: Experimental cpx/melt partitioning of 24 trace elements. *Contr. Mineral. Petrology* 113, 1–8.

Hellebrand E., Snow J.E., Dick H.J.B. & Hofmann A.W. 2001: Coupled major and trace elements as indicators of the extent of melting in mid-ocean-ridge peridotites. *Nature* 410, 677–681.

Iancu V., Berza T., Seghedi A., Gheuca I. & Hann H.-P. 2005: Alpine polyphase tectono-metamorphic evolution of the South Carpathians: A new overview. *Tectonophysics* 410, 337–365.

Ianovici V., Vlad S., Borcos M. & Bostinescu S. 1977: Alpine porphyry copper mineralization of West Romania. *Mineralium Depos.* 12, 307–317.

Janković S. 1997: The Carpatho–Balkanides and adjacent area: a sector of the Tethyan Eurasian metallogenetic belt. *Mineralium Depos.* 32, 426–433.

Jovanović M., Downes H., Vaselli O., Cvetković V., Prelević D. & Pécskay Z. 2001: Paleogene mafic alkaline volcanic rocks of East Serbia. *Acta Vulcanol.* 13, 159–173.

Karamata S., Knezević V., Pécskay Z. & Djordjević M. 1997: Magmatism and metallogeny of the Ridanj–Krepoljin belt (eastern Serbia) and their correlation with northern and eastern analogues. *Mineralium Depos.* 32, 452–458.

Kelemen P.B., Dick H.J.B. & Quick J.E. 1992: Formation of harzburgite by pervasive melt-rock reaction in the upper mantle. *Nature* 358, 635–644.

Kelemen P.B., Hart S.R. & Bernstein S. 1998: Silica enrichment in the continental upper mantle via melt/rock reaction. *Earth Planet. Sci. Lett.* 164, 387–406.

Kräutner F. 1969: Magmatites finales alcalines quaternaires dans la partie NE du massif de Poiana Rusca. *Rev. Roum. Géol. Géophys. Géogr., Sér. Géol.* 13, 47–67.

Kräutner H.G. 1997: Alpine and pre-Alpine terranes in the Romanian Carpathians and Apuseni Mountains. *IGCP Project No. 276. Ann. Geol. Pays. Hellén.* 37, 331–400.

Manning C.E. 2004: The chemistry of subduction-zone fluids. *Earth Planet. Sci. Lett.* 223, 1–16.

Marchev P., Arai S., & Vaselli O. 2006: Cumulate xenoliths in Oligocene alkaline basaltic and lamprophyric dikes from the eastern Rhodopes, Bulgaria: Evidence for the existence of layered plutons under the metamorphic core complexes. *Geol. Soc. Amer., Spec. Pap.* 409, 237–258.

Marchev P., Arai S., Ishida Y., Shirasaka M. & Downes H. 2008: Trace element and isotopic composition of mafic and ultramafic cumulate xenoliths in alkaline basalts from the Eastern Rhodopes, Bulgaria: Inferences on deep processes under the metamorphic core complexes. *IOP Conf. Series: Earth and Environmental Science* 2, 012015.

McDonough W.F. & Sun S.S. 1995: The composition of the Earth. *Chem. Geol.* 120, 223–253.

McInnes B.I.A., Gregoire M., Binns R.A., Herzig P.M. & Hannington M.D. 2001: Hydrous metasomatism of the sub-arc mantle, Lihir, Papua New Guinea: petrology and geochemistry of fluid metasomatised mantle wedge. *Earth Planet. Sci. Lett.* 188, 169–183.

McKenzie D. & O'Nions R.K. 1991: Partial melt distributions from inversion of rare earth element concentrations. *J. Petrology* 32, 1021–1091.

Norman M.D. 1998: Melting and metasomatism in the continental lithosphere: laser ablation ICPMS analysis of minerals in spinel lherzolites from eastern Australia. *Contr. Mineral. Petrology* 130, 240–255.

Pearce N.J.G., Perkins W.T., Westgate J.A., Gorton M.P., Jackson S.E., Neal C.R. & Chenery S.P. 1997: A compilation of new major and trace element data for NIST SRM 610 and NIST SRM 612 glass reference materials. *J. Geostand. Geoanalysis* 21, 115–144.

Rădulescu D. & Săndulescu M. 1973: The plate-tectonics concept and geological structure of the Carpathians. *Tectonophysics* 16, 155–161.

Rehfeldt T., Foley S.F., Jacob D.E., Carlson R.W. & Lowry D. 2008: Contrasting types of metasomatism in dunite, wehrlite and websterite xenoliths from Kimberley, South Africa. *Geochim. Cosmochim. Acta* 72, 5722–5756.

Ringwood A.E. 1958: Constitution of the mantle. *Geochim. Cosmochim. Acta* 15, 195–212.

Russo-Săndulescu D. & Berza T. 1979: Banatites from the western part of the Southern Carpathians (Banat). *Rev. Roum. Géol. Géophys. Géogr., Sér. Géol.* 23, 149–158.

Russo-Săndulescu D., Berza T., Bratosin I. & Ianc R. 1978: Petrological study of the Bocsa Banatitic massif (Banat). *Dări de Seăma ale Institutului de Geologie si Geofizica* 64, 1, 105–172.

Santos J.F., Scharer U., Gil Ibarguchi J.I. & Girardeau J. 2002: Genesis of pyroxenite-rich peridotite at Cabo Ortegal (NW Spain): Geochemical and Pb–Sr–Nd isotope data. *J. Petrology* 43, 17–43.

Schmid S.M., Bernoulli D., Fügenschuh B., Matenco L., Schefer S., Schuster R., Tischler M. & Ustaszewski K. 2008: The Alpine–Carpathian–Dinaridic orogenic system: correlation and evolution of tectonic units. *Swiss J. Geosci.* 101, 139–183.

Smith D., Riter J.C.A. & Mertzman S.A. 1999: Water–rock interactions, orthopyroxene growth, and Si-enrichment in the mantle: evidence in xenoliths from the Colorado Plateau, southwestern United States. *Earth Planet. Sci. Lett.* 165, 45–54.

Stosch H.G. 1982: Rare earth element partitioning between minerals from spinel peridotite xenoliths. *Contr. Mineral. Petrology* 78, 166–174.

Sun S.S. & McDonough W.F. 1989: Chemical and isotopic systematics of oceanic basalts; implications for mantle composition and processes. In: Saunders A.D. & Norry M.J. (Eds.): Magmatism in the ocean basins. *Geol. Soc. London, Spec. Publ.* 42, 313–345.

Tschegg C., Ntaflos T., Seghedi I., Harangi S., Kosler J. & Coltorti M. 2010: Paleogene alkaline magmatism in the South Carpathians (Poiana Ruscă, Romania): Asthenospheric melts with geodynamic and lithospheric information. *Lithos* 120, 393–406.

von Cotta B. 1864: Erzlagerstatten im Banat und in Serbien. *W. Braumuller*, Wien, 1–105.

Wilshire H.G. & Shervais J.W. 1975: Al-augite and Cr-diopside ultramafic xenoliths in basaltic rocks from western United States. *Phys. Chem. Earth* 9, 257–272.

Wulff-Pedersen E.N., Neumann E.-R. & Jensen B.B. 1996: The upper mantle under La Palma, Canary Islands: formation of Si–K–Na-rich melt and its importance as a metasomatic agent. *Contr. Mineral. Petrology* 125, 113–139.

Wulff-Pedersen E.N., Neumann E.-R., Vannucci R., Bottazzi P. & Ottolini L. 1999: Silicic melts produced by reaction between peridotite and infiltrating basaltic melts: ion probe data on glasses and minerals in veined xenoliths from La Palma, Canary Islands. *Contr. Mineral. Petrology* 137, 59–82.

Xu Y.G., Menzies M.A., Vroon P., Mercier J.-C. & Lin C.Y. 1998: Melt percolation-reaction atop the plume: evidence from poikiloblastic spinel harzburgite xenoliths from Boree (Massif Central, France). *Contr. Mineral. Petrology* 132, 65–84.

Zindler A. & Jagoutz E. 1988: Mantle cryptology. *Geochim. Cosmochim. Acta* 52, 319–333.